2
MFI: A Case Study of Zeolite Synthesis

Ramsharan Singh and Prabir K. Dutta
The Ohio State University, Columbus, Ohio, U.S.A.

I. INTRODUCTION

Zeolite synthesis occurs by a hydrothermal process with reagents being a silica source, an alumina source, a mineralizing agent such as OH^- or F^-, and, for higher Si/Al ratio zeolites, organic molecules as structure-directing agents. The role of inorganic metal cations, such as Na^+ or K^+, is quite profound. A schematic of the zeolite growth process is shown in Fig. 1 (1). The complexity of the process, including the presence of numerous soluble species, an amorphous phase, polymerization and depolymerization reactions, makes the synthesis susceptible to physical effects such as stirring, aging, and order of reagent addition (2). Several independent processes are occurring in the medium, including nucleation of various structures, crystallization as well as dissolution of metastable phases. It is commonly observed that the conversion of the composition (gel or solution) to crystals is quite rapid once the crystallization process gets started. This suggests that nucleation is the rate-limiting step and is consistent with studies that report addition of seed crystals decrease the induction time (2). Tezak suggested several decades ago that rather than viewing the synthesis process as nucleation and crystallization, at least four subsystems be considered: (a) formation of simple and polymeric

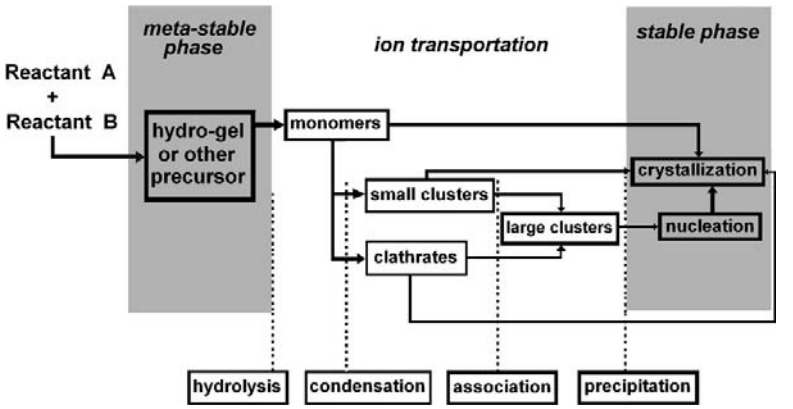

Fig. 1 A schematic representation of zeolite crystallization process. (From Ref. 1.)

aluminosilicates, (b) aggregation of these complexes to form embryo, (c) nucleation as aggregate formation with a well ordered core and micelle formation (primary particles), and (d) aggregation of primary particles via oriented aggregation (3). Flanigen has elaborated on these concepts further (4).

Starting with the physical form of the reactants and their precise chemical composition to the synthesis conditions, each of these parameters can have a profound influence on the resulting zeolite crystallization. One way to think about zeolite crystallization is to view it as a process with multiple pathways. Pathways for a specific framework may be intertwined with another path that leads to a different zeolite framework. Thus, minor perturbations can lead to "lane switching" and formation of unanticipated crystal topologies. Such path overlap and multiple pathways make it difficult to carry out designed zeolite synthesis routes. Most of the advances have come in this field from trial-and-error discoveries, and development of important empirical information has been the basis of further development.

Considering that there are more than 100 frameworks, each with multiple synthetic procedures, it is important to ask what is the optimal way to learn about zeolite synthesis. Several possible options exist, such as:

Cataloging all the possible recipes for formation of different zeolites

Defining composition fields of different zeolites, making clear the overlap and boundaries

Contrasting growth patterns of different zeolites

Examining a single zeolite synthesis from different perspectives

In this chapter, we have taken the approach of focusing on a single framework, MFI, and examining the literature related to its crystallization. Arguably, this framework is the most studied of all zeolites, and examining its growth from different perspectives provides a comprehensive picture of zeolite crystallization. Obviously, some of the specific details are peculiar to MFI-type frameworks and not readily extendable to other systems. Yet the conclusions that can be drawn from the data should be more generally applicable.

The crystallization of ZSM-5 was first reported in 1978 (5). ZSM-5 typically crystallizes in the Pnma orthorhombic space group with lattice constants $a = 20.1$, $b = 19.9$, and $c = 13.4$ Å. The framework density of Si + Al atoms is 17.9 per 1000 Å^3. Fig. 2a shows the skeletal diagram of (100) face of ZSM-5, where the 10-membered ring apertures are the entrances to the sinusoidal channels. Fig. 2b shows the channel structure of ZSM-5. There are two channel systems in ZSM-5: a straight channel running parallel to (010) with 10-ring openings of 5.4 × 5.6 Å, and a sinusoidal channel parallel to the (100) axis with 10-ring openings of dimension 5.1 × 5.5 Å (6,7). The O-T-O bond angles vary between 105° and 113° with an average value

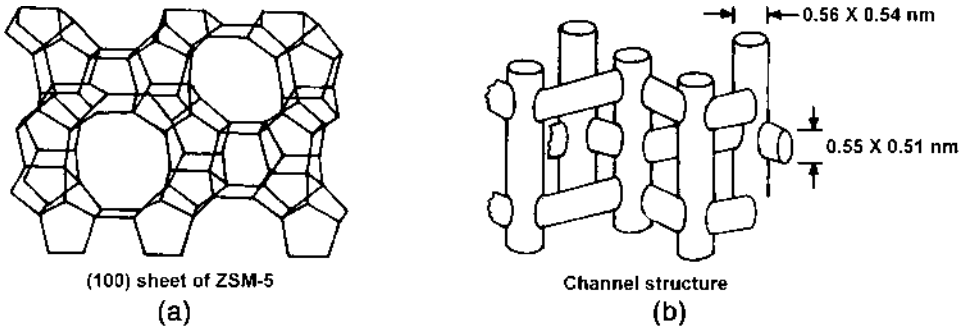

Fig. 2 (a) Skeletal diagram of the (100) face of ZSM-5. (b) Channel structure of ZSM-5.

of 109 ± 2°. Among the T-O-T angles, two almost linear bonds are observed at 176.2° and 178° (8). The tetrapropylammonium ion (TPA), typically used for synthesizing the MFI framework, is located in the intersection of the two channels, with a conformation different from that in TPA Br (9).

The mineral counterpart of ZSM-5, mutinaite, was recently discovered at Mt. Adamson, Northern Victoria Land, Antarctica. Its composition was found to be $Na_{2.76}K_{0.11}Mg_{0.21}$-$Ca_{3.78}Al_{11.20}Si_{84.91}60\ H_2O$ with an orthorhombic space group (Pnma), with a = 20.201(2), b = 19.991(2), and c = 13.469(2) Å. The Si-Al in the framework was disordered, and large distances between ions in the channels and framework oxygens were noted (10).

The completely siliceous form of ZSM-5, silicalite, exhibits hydrophobicity and can extract organic molecules from water streams. The defect hydroxyl groups in silicalite cause residual hydrophilicity, which can be completely absent in fluoride-silicalite, and exhibits extreme hydrophobic behavior, adsorbing <1 wt % water at 20 Torr at 25°C. These crystals of density 1.7 g/mL will float on water (11,12).

The overall plan of the chapter is as follows. We examine first how reactant composition influences crystallization, with particular focus on the role of inorganic and organic cations as well as organic molecules. The role of physical conditions, such as temperature and crystallization in the presence of seeds, is discussed. Synthesis in the presence of fluoride ions and organic solvents is contrasted with conventional hydrothermal synthesis. This section demonstrates that for ZSM-5 synthesis, inorganic cations define a very narrow composition field, which can be significantly expanded by the use of organic species.

The diversity of the crystals that can be synthesized is the focus of the second section. Besides a wide range of chemical compositions, MFI can be obtained as nanocrystals, single crystals, intergrowths, membranes, and thin films.

The third section focuses on morphology of the crystals and how it is influenced by variation of the synthesis parameters.

The mechanism of crystal growth from the macroscopic to the molecular level is the focus of the final two sections. There have been several reviews regarding synthesis of zeolites and molecular sieves (13–16). The evolution of molecular sieve zeolite technology for the period up to the early 1980s has been summarized (11).

II. COMPOSITIONAL INFLUENCE ON CRYSTALLIZATION

We summarize below various compositional dependences on crystal growth, including the role of Si, Al, inorganic and organic species, temperature, OH^- versus F^-, water-organic solvents, and seeded growth. The objective here is to address the following questions:

What range of compositions will result in the MFI structure and how is this controlled by the cations present in the mixture?

What role do organic cations play in extending the range of compositions and for what reasons?

What is the correlation between structure of the organic species and the MFI framework?

How does temperature influence the crystallization process?

What are the comparisons between the conventional OH^--based synthesis systems and F^-?

How does the synthesis result change as water is replaced by organic solvents?

What does a seeded system offer for crystallization?

What are unusual methods of synthesis?

We answer these questions in a systematic manner and at the end of each section summarize the important features.

A. Reactants

1. Alkali Metal and Mixed Ion Systems with Tetrapropylammonium Ion (TPA)

Organic-free ZSM-5 synthesis has been reported for the composition $aSiO_2/Al_2O_3/bNa_2O/1500\ H_2O$ (a = 20–∞, b = 4.5–10) in the temperature range of 423–463 K. For $a < 30$, mordenite with traces of ZSM-5 was formed, whereas for $a \geq 60$, α-quartz, ZSM-5, and mordenite were formed. At $a = 40$ and b = 4.5–6.0, pure ZSM-5 was observed, the structural stability of which was lower than that of a similar sample made in the presence of organics. The reason for the instability was attributed to excess sodium occluded within the framework (17).

The synthesis of ZSM-5 from high-silica systems in the presence of alkali cations lithium, sodium, and potassium has been systematically studied by several groups (18–22). Crystallization of ZSM-5 was not observed in the case of Li and K, and only in a very narrow region in the case of Na. In the bicationic alkali system, e.g., in the case of Li, Na, a mixture of ZSM-5 and mordenite was obtained, whereas in the case of Li, K, there was no crystallization, and in the case of Na, K, pure ZSM-5 formed in a narrow composition range and no crystallization occurred in the case of Li, K. However ZSM-5 crystallized in the presence of TPABr in all cases. The fact that TPA did not direct ZSM-5, only silicalite, but did do so in the presence of alkali cations was interpreted to mean that alkali cations are necessary to stabilize Al-containing "5-1" SBU units (18).

Recently it was reported that, in the absence of TPA, the crystallization of ZSM-5 occurred in a narrow composition range in the presence of potassium, though the authors cautioned that the presence of organic impurities may have caused the crystallization of ZSM-5 (20).

Based on a systematic study of MFI-type zeolites starting from template-free reaction gels, it was reported that either MFI- or MOR-like zeolites can be prepared from the same synthesis gel by changing either temperature or crystallization time. An upper limit for the incorporation of silica in the MFI framework was observed, regardless of the silica-to-alumina ratio of the starting gel, the resulting crystals having Si/Al ratios ranging from 12 to 29 (21).

The (Li, Na)-, Na-, and (Na,K)ZSM-5 zeolites have been prepared in hydrothermal conditions at 443 K from highly dense gels of compositions $aM_2O\ bAl_2O_3\ 150SiO_2\ 490H_2O$ with M = Li, Na, or K; $0.9 \leq a \leq 8.82$ and $1.66 \leq b \leq 15$ (22). In a narrow range of compositions, (Li, Na)ZSM-5 self-bonded pellets were formed from the composition with $8 \leq a \leq 9$ and $14 \leq b \leq 16$. The approximately 4 μm ZSM-5 crystallites were embedded in an amorphous gel formed of $LiAlO_2$. Figure 3 shows the crystallization curves and somewhat surprisingly, it was found that the (K, Na) system has the shortest induction period, whereas the (Na) system shows the longest induction period, with (Li, Na) being intermediate (22). K^+ and Na^+ promote dissolution of quartz compared with Mg^{2+} and Li^+, and this observation has been used to hypothesize that K^+/Na^+ are more effective in polymerization/depolymerization reactions of silicates present during the synthesis (14).

The range of compositions from which ZSM-5 can be synthesized is considerably extended by inclusion of TPA. Synthesis of ZSM-5 in Na^+-TPA, Li^+-TPA, and NH_4^+-TPA systems has been reported (23,24). In the NH_4^+-TPA system, crystals as large as 350 μm were formed (23). No dependence of crystallization rate on Li^+, K^+ was noted for systems with a high TPA content (24). Based on nuclear magnetic resonance (NMR) studies, Nagy et al.

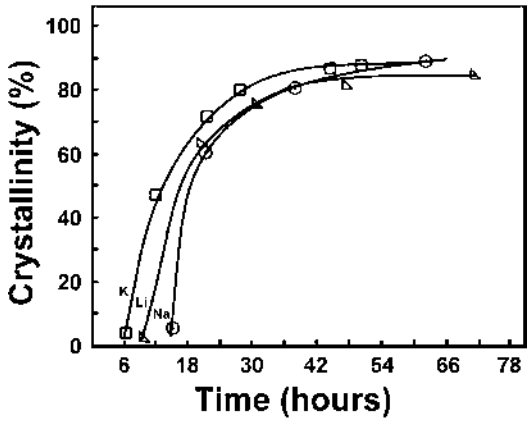

Fig. 3 Crystallization curves of the (M,Na)ZSM-5 zeolites obtained from the gels 8.8 M_2O|15 Na_2O|5 TPABr|2.5 Al_2O_3|150 SiO_2|490 H_2O at 443 K. (From Ref. 22.)

concluded that alkali cations were incorporated into the zeolite channels in the early part of the crystallization as hydrated units acting as counterions to $(Si\text{-}O\text{-}Al)^-$, and later as less hydrated counterions to defective $Si\text{-}O^-$ groups (24). A nucleation mechanism at the gel–liquid interface and crystal growth through liquid phase transport of nutrients was proposed (24). The number of TPA ions per unit cell was reported to be between 3.8 and 4.0, indicating the presence of TPA in all the four-channel interactions per unit cell (24). It was found that TPA incorporation into the zeolite framework began with crystal growth (25). The enhanced structure-directing ability of TPA has been correlated with its geometry and charge (26).

The role of alkali and ammonium cations in governing nucleation and growth processes of (M^I)ZSM-5 zeolites formed within the $(Na_2O, M_2O)\text{-}(Pr_4N)_2O\text{-}Al_2O_3\text{-}SiO_2\text{-}H_2O$ synthesis mixtures (M^I = Li, Na, NH_4, K, Rb, Cs) has been studied (27,28). Morphology, size, chemical composition, and homogeneity of the (M^I)-ZSM-5 crystallites depended on the competitive interaction between Pr_4N^+ or alkali cationic species and aluminosilicate anions at the early stages of the nucleation process. Flanigen has proposed that the electrostatic interaction between cations and aluminosilicate species is dependent on the cation charge density (Ze/r, where Z is charge and r is ionic radius) and follows the order Ca > Sr > Ba > Li > Na > K > Rb > Cs. Alkali ions have been proposed to help aggregate sol particles (11). Intrinsic properties of the alkali cations, including their size, structure-forming or structure-breaking role toward water, and salting-out power, were found to be important. Fig. 4 shows that structure-breaking cations such as K^+, Rb^+ or Cs^+ favored the formation of large (15–25 μm) single crystals or twins, whereas structure-forming cations (Li^+, Na^+) yielded Si-rich crystallites distributed within the 5- to 15 μm range. The latter crystals were coated with numerous small (1 μm) Al-richer crystallites formed by a secondary nucleation process from the Si-deficient gel. As a result, K, Rb, and Cs ZSM-5 zeolites appeared homogeneous in composition whereas Li and Na polycrystalline aggregates showed an apparent Al-enriched outer rim (27). In the presence of NH_4^+ ions, large single crystals of ZSM-5 having an Al-deficient core and an Al-rich outer shell, as well as small Si-rich crystallites stemming from a delayed nucleation process, were reported. The particular role of NH_4^+ was explained in terms of its preferential interaction with aluminate rather than silicate during nucleation (27).

The synthesis of zeolite TPA-ZSM-5 with $(NH_4)_2O/Al_2O_3 = 38$ and different amounts of Li_2O, Na_2O, or K_2O has been studied (28). The growth of the crystals as a function of time

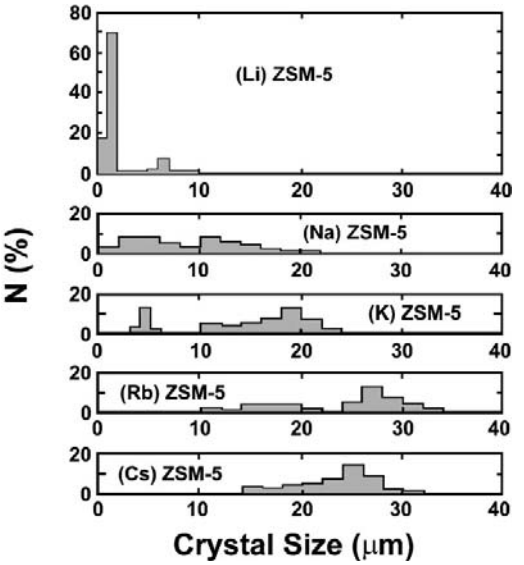

Fig. 4 Crystal size distribution of the various (M)ZSM-5 zeolites determined from scanning electron micrographs. (From Ref. 27.)

showed an increment of the size of the crystals when alkali metal oxide was added. With Li_2O uniform, large, lath-shaped crystals of ZSM-5 $\sim 140 \pm 10$ μm in length were obtained. The time of nucleation was long when $(NH_4)_2O$ was used with TPA and decreased when alkali was added to the system.

Crystallization of Al-free NH_4-ZSM-5 has been studied in an alkali-metal free system with seeding experiments (29). The crystallization of TPA-ZSM-5 has been reported using ammonium cations instead of alkali metal cations (30,31).

ZSM-5 has been synthesized from sodium tetrapropylammonium aluminosilicate and silicate gels (32). The effects of varying the ratio of Si/Al and alkalinity in the starting gels and the reaction temperature were studied. The alkalinity was found to affect the rate of nucleation more than the rate of crystal growth. An optimal alkalinity was found for synthesis of ZSM-5 as shown in Fig. 5 and was related to the Si/Al ratio of the reactants.

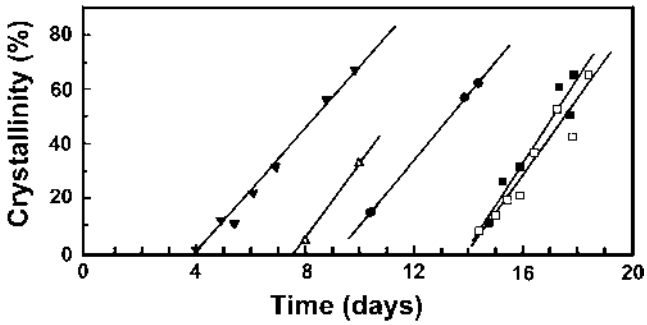

Fig. 5 Influence of alkalinity on ZSM-5 crystallization. Temperature = 367 K. ■ SiO_2/Al_2O_3 = 140, H_2O/OH^- = 450; ▼ SiO_2/Al_2O_3 = 140, H_2O/OH^- = 225; ● SiO_2/Al_2O_3 = 140, H_2O/OH^- = 112; □ SiO_2/Al_2O_3 = 90, H_2O/OH^- = 450; △ SiO_2/Al_2O_3 = 90, H_2O/OH^- = 225. (From Ref. 32.)

Addition of a small amount of certain oxyanions of group VA and VIIA (such as perchlorate, phosphate, arsenate, chlorate, and bromate) significantly enhanced the nucleation and crystalliation process of ZSM-5 (33). For example, the time taken to obtain fully crystalline ZSM-5 with different promoters followed the order: ClO_4^- (7 h) < PO_4^{3-} (8 h) < AsO_4^{3-} (14 h) < none (48 h). With phosphate as promoter, it was noted that the quality of the material (crystallinity and adsorption/catalytic properties) was comparable with, if not better than, that prepared in the absence of promoter. The crystallite size of ZSM-5 samples prepared in the presence of phosphate as promoter was smaller with a narrower particle size distribution.

Zeolite crystals have been grown in microgravity environment (10^{-3}–10^{-6} g) (34,35). The flight crystals grown on the space shuttle from silica gel had intergrown disk morphology and were larger than the spherulitic aggregates of small elementary crystals observed for the terrestrial/control samples. It was concluded that the nucleation rate of ZSM-5 was reduced in microgravity (35).

Free energy considerations indicated that the transformation of quartz to silicalite was unfavorable (4.1 kJ/mol SiO_2), whereas in the presence of TPA it was favored (−3.8 kJ/mol SiO_2). The exothermic enthalpic contribution arose from the tight fit of the TPA within the intersecting channels of silicalite, whereas the increasing entropic contribution came from the disordering of water molecules external to the framework upon encapsulation of TPA in the zeolite (14).

Based on the above results, the insights that can be obtained are as follows:

Crystallization of ZSM-5 is possible only in a very limited range with Na^+, to some extent with K^+, but not at all with Li^+. However, for bicationic systems with Na^+ as one of the ions, synthesis is possible.

Presence of TPA extends the range of compositions over which MFI crystals can be formed.

Alkali metal cations when present in the TPA system influence the morphology and the distribution of Si/Al in the framework. The alkali ions compete with the TPA–aluminosilicate interactions during the nucleation stage. Structure-breaking cations such as K^+, Rb^+, or Cs^+ favor the formation of large (15–25 μm) single crystals or twins.

The role of NH_4^+ is quite distinct from that of the alkali metal ions because of their preferential interaction with aluminate rather than silicate ions in the nucleation stage. In the presence of NH_4^+ ions, large single crystals of ZSM-5 having an Al-deficient core and an Al-rich outer shell, as well as small Si-rich crystallites stemming from a delayed nucleation process, are formed. Crystal size increases when alkali hydroxide is added to an (NH_4)O-TPA-ZSM-5 system. Ammonium ions also tend to increase nucleation times as compared with alkali cations.

For every Si/Al ratio, there appears to be an optimal alkalinity. The influence of alkalinity was more on nucleation rate than crystal growth.

Certain oxyanions (such as PO_4^{3-}) promote zeolite growth.

2. Quarternized Ions (Other than TPA)

The role of various organic molecules as structure-directing agents in the synthesis of molecular sieves has been reviewed (36). The number of organic species in whose presence ZSM-5 has been synthesized is quite large (36). Table 1 lists some of the organic molecules used in ZSM-5 synthesis and shows that there is no common feature between these molecules, suggesting that strict templating is not playing a role in the synthesis in

Table 1 Organic Molecules Used for Synthesis of ZSM-5

Tetrapropylammonium	Di-*n*-propylamine
Tetraethylammonium	1,5-Diaminopentane
Tripropylamine	1,6-Diaminohexane
Ethyldiamine	Morpholine
Propanolamine	Pentaerythritol
Ethanolamine	Dipropylenetriamine
Methyl quinuclide	Dihexamethylenetriamine
NH_3 + alcohol	Triethylenetetramine
Alcohols	Diethylenetetramine
Glycerol	1-Alkyl-4-azonibicyclo[2,2,2]octane-4-oxide halide
n-Propylamine	Hexanediol
Di-*n*-butylamine	Propylamine

Source: Ref. 36.

most cases. Rather, with the appropriate gel chemistry, the presence of organics aids in the synthesis.

The role of organic molecules in the synthesis of zeolites can be in various forms: space filling, structure directing, and templating. In the case of ZSM-5, most of the organic molecules can be considered to be space fillers, except for TPA. TPA can be thought of as structure directing, since it promotes the synthesis of MFI over a wide range of compositions and is also entrapped in the channels of the zeolite. There are very few examples of true templating, the best example being $C_{18}H_{36}N^+$ in the synthesis of ZSM-18. The tri-quat molecule fits into the ZSM-18 cage with the same C_3 rotational symmetry of the cage, and its rotational mobility is completely restricted (37).

Because of the unique role played by TPA for MFI synthesis as described above, there has been a number of studies on the influence of other tetraalkylammonium (TAA) cations (38,39). Tetramethylammonium (TMA) is hydrophilic, whereas TPA is hydrophobic because of the longer propyl chains, whereas tetraethylammonium (TEA) is intermediate in behavior. Thus, silicate ions should preferably displace the water molecules around TPA over TMA (14). The role of TMA, TEA, and tetrabutylammonium (TBA) cations in the presence of either lithium or potassium ions has been examined (38). In presence of K^+ and TEABr, the main zeolitic phase was ZSM-5. The induction periods were slightly influenced, while the crystallization rate increased with increasing TEA concentration. In the presence of Li^+ ions, the induction period decreased, while the crystallization rate also increased with increasing TEA concentration. However, TMA cations directed the formation of other zeolites. In the presence of Li^+ ions, ZSM-5 and ZSM-39 were formed. In the presence of K^+ ions, ZSM-5 was the main zeolitic phase at low TMA concentration, while at high TMA concentrations, ZSM-39 and ZSM-48 were formed.

ZSM-5 has been prepared at 443 K from clear solutions of general composition SiO_2 / $0.0004Al_2O_3/0.30Na_2O/a$TAABr (or TAAOH)/$40H_2O$ with a = 0.03–0.16 and TAA = TEA, TPA, or TBA (39). The number of defects in the crystal of the type Si-O-M (M = H, Na, TPA) were higher than that of a hydrogel synthesis system.

Energy calculations have been carried out to explain the stabilization achieved by the occlusion of TAA and other cations in ZSM-5 (40–42). The zeolite was treated as a rigid framework, whereas the TAA cations were allowed to be flexible (40). Nonbonded intra template, template–template, and template–zeolite interactions were considered, and calculations were performed for TAA loadings of 1, 3, and 4 cations per zeolite unit cell. At the level

of 1 TAA per unit cell, the stabilization energy increased monotonically with the C/N ratio of the cation. Stabilization energies as a function of TAA ions occluded in ZSM-5 and ZSM-11 are compared in Fig. 6 (40). For four TAA cations per unit cell, the stabilization energy increased to a maximum for TPA and then declined in progressing to TBA. Reducing the loading of TBA to three cations per unit cell increased the stabilization energy relative to that obtained for four cations per unit cell, but the stabilization energy was still less than that achieved with four TPA cations per unit cell. Increasing the length of the alkyl chain led to an increase in organic-zeolite nonbonded interactions and hence the stabilization of the zeolite. In the case of TBA, an energetically unfavorable configuration, as well as repulsive interactions between the methyl groups, led to destabilization (40).

Several organic structure-directing agents that were variations of a 4,4′-trimethylene-bis(*N*-methyl, *N*-R_1-piperidinium) moiety have been used for the synthesis of pure-silica molecular sieves (43). When R_1 was pentyl or hexyl, MFI was crystallized, suggesting that each structure-directing molecule spanned two channel interactions. The role of the optimal organic–zeolite interactions in stabilizing ZSM-5 was also evidenced here, since if R_1 is butyl or heptyl, the MFI structure was not formed, and phases BEA and BTW, respectively, were obtained (43).

Patarin et al. synthesized ZSM-5 with TPA^+F^-, $(C_3H_7)_2NH_2^+F^-$ (DIPA), and $(C_3H_7)_3NH^+F^-$ (TRIPA), and based on enthalpy measurements concluded that DIPA and TRIPA stabilize the organic–inorganic composites less than TPA. This was because of the tight fit of the TPA at the channel intersections (44).

Tetrapropylammonium, ethanoltripropylammonium, and diethanoldipropylammonium cations have been used as structure-directing agents for the synthesis of pure-silica, MFI-type zeolites. Ethanoltripropylammonium cation directed the formation of silicalite but at a slower rate than tetrapropylammonium cation. Diethanoldipropylammonium needed the presence of either seeds or a small amount of tetrapropylammonium to form silicalite. All ethanolalkyl-ammonium molecules were occluded intact in the zeolite pores. It was concluded that control of

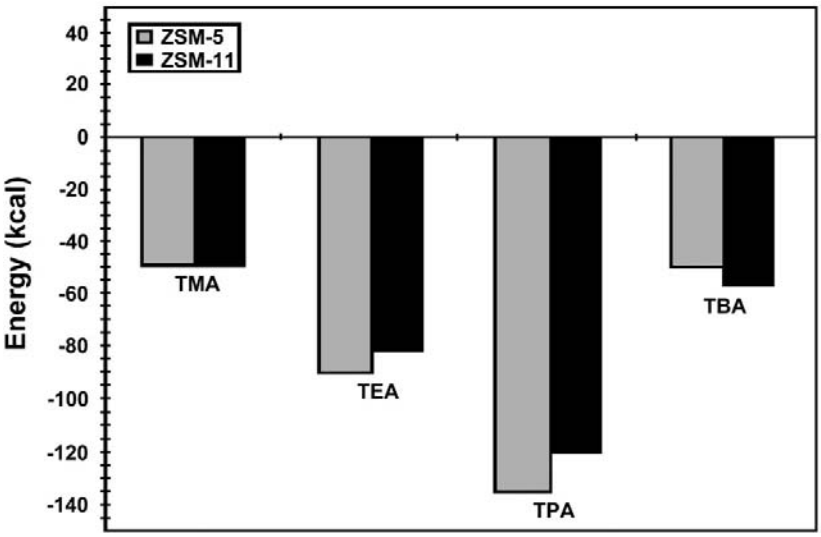

Fig. 6 Stablization energy for tetraalkylammonium cations occluded in ZSM-5 and ZSM-11 at an occupancy of four cations per unit cell. All energies are in kcal per unit cell. (From Ref. 40.)

the hydrophobicity of the organic structure-directing agent was necessary for the synthesis of pure-silica zeolites (45).

The following insight can be gained from these studies:

True templating in zeolite formation is rare.

TMA only forms ZSM-5 over a narrow range of concentrations and directs formation of ZSM-39 and ZSM-48. TEA is more favorable for ZSM-5 formation.

Calculations show that at a level of 1 TAA^+ per unit cell, the stabilization energy increases monotonically with the C/N ratio of the cation. For four TAA^+ cations per unit cell, the stabilization energy increases to a maximum for TPA and then declines in progressing to TBA. Increase in organic–zeolite nonbonded interactions favors zeolite stabilization.

Simple modifications on one of the propyl groups in TPA is enough to disrupt the organic–inorganic interactions and reduce the rate of crystal formation.

3. Amines and Other Structure-Directing Agents

Extensive studies have been done with amines as structure-directing agents. The crystallization of high SiO_2/Al_2O_3 zeolites in the presence of various diamines at pH < 12 has been examined (46,47). It was shown that, as the number of CH_2 units separating the amine functional groups increases, the zeolite type changes from FER to MFI to MEL (46). The MFI structure has been obtained only with diamines having C_4, C_5, C_6, and C_{12} carbon atoms. However, by changing composition, ZSM-5 was crystallized from diamines having C_2, C_3, C_4, and C_6 carbon atoms (47). It was shown that crystallization rate decreased with increase in the linear dimension of the amine. The charge neutralization occurred by protonated amines, since the Na^+ content was less than one per unit cell.

Several other organic molecules, such as 1,6-hexane-diol, 1-propanol, 1-propane amine, pentaerythritol, and piperazine, have been used in the synthesis of ZSM-5 and silicalite, and acted as void fillers, with little structure-directing ability (48–52). Synthesis of ZSM-5 using 1,6-hexanediol as a structure-directing agent has been reported in a vigorously stirred system at 425, 433 and 443 K, and the data analyzed with population balance models (49). The autocatalytic model with release of nonuniformly distributed nuclei provided a good fit of the experimental data. ZSM-5 has been synthesized in the presence of tetra-, tri-, and dipropylammonium fluoride species (53).

The use of tributylamine (TBA) composition resulted in a phase rich in ZSM-5, whereas the use of tripropylamine (TrPA) yielded ZSM-11-rich phase for the same compostion (25). Using a mixture of TrPA and *n*-propyl bromide (PrBr), a pure ZSM-5 phase was reported. It was suggested that TPA cations were formed in traces and helped the nucleation process.

The synthesis of silicalite-1 in presence of diethylamine (DEA) has been reported (54). The formation of DEA-silicalite-1 is favored by static conditions, high DEA concentrations, and low temperature (393 K), but the structure-directing property of DEA was marginal. Hexane-1,6-diamine (HEXDM) was found to be a good void filler for the MFI framework and synthesis of silicalite-1 (55,56). Silicalite-1 made in the presence of HEXDM formed only at low temperatures, static reaction conditions, and high $HEXDM/SiO_2$ mole ratios, suggesting reasonably narrow and exacting conditions for the growth of these open framework materials. ZSM-48 and eventually quartz were the competing frameworks at higher temperatures (55). For synthesis of MFI structure with HEDXM at high temperatures, Al was necessary (56).

The crystallization of alkali-metal-free silicalite-1 from the reaction mixture containing piperazine, silica, water, and various quaternary ammonium ions has been reported under static and stirred conditions (51,52).

A correlation between dipole moment, ionization potential, maximal length, and bond angle between propyl groups and the kinetics of ZSM-5 zeolite has been made for propylamine, dipropylamine, tripropylamine, and tetrapropylammonium bromide (26). The conclusions were that the polarity of the organic molecule (characterized by dipole moment) determined the induction period. The molecules with higher dipole moment had shorter induction periods, as for propylamine. The low dipole moment and the geometrical configuration of tripropylamine (angle between the propyl groups is 117° whereas the angle between linear and sinusoidal channels is 110°) was proposed to be the reason for the longer period of nucleation and the slower crystallization process.

The following insight can be gained from these studies:

Simple secondary and tertiary amines will direct MFI synthesis under a narrow range of conditions. Tripropylamine directs ZSM-11, but in the presence of PrBr makes pure ZSM-5, presumably due to in situ formation of TPA.

α,ω diamines will direct ZSM-5 formation under restricted compositions and crystallization rate decreases with the linear dimension of the molecule.

Correlations have been made between the structure-directing abilities of a series of propylamine-containing molecules and dipole moment, ionization potential, and their geometrical characteristics. The molecules with higher dipole moment had a shorter induction period.

B. Temperature

Temperature variations have been used to study the growth process, optimize yields, and alter morphology.

The crystallization of ZSM-5 at temperatures of 423, 438 and 453 K for a reactant composition $30Na_2O/68TPA_2O/Al_2O_3/111SiO_2/4000H_2O/25H_2SO_4$ has been reported (57). Analysis of the kinetic data suggests that the growth mechanism was independent of temperature (57). It was observed that induction time decreased and crystallization rate increased on increasing temperature, as shown in Fig. 7. Similar conclusions were reached for ZSM-5

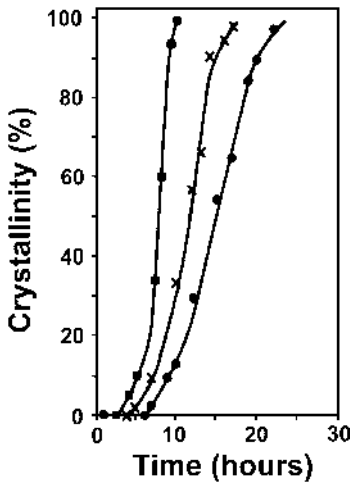

Fig. 7 Crystallization curves for ZSM-5 at 423 (●), 438 (×), and 453 (■) K using TPABr. (From Ref. 57.)

synthesized from a gel with initial mole composition of $33Na_2O/44R/Al_2O_3/100SiO_2/4000H_2O/25H_2SO_4$ (R = 1,2-diaminoethane, 1,3-diamonopropane, 1,4-diaminobutane, 1,6-diaminohexane, and TPABr) at temperatures of 423, 438 and 453 K (46,47). Organic-free crystallization of ZSM-5 (17) using a gel composition of $40SiO_2/Al_2O_3/4.5Na_2O/1500H_2O$ at temperatures of 423, 443, and 463 K also exhibited increased rate of crystallization with temperature. For prolonged crystallization at a particular temperature (373 K), the crystallite size was found to grow from 1 to 4 μm, indicating an Ostwald ripening phenomenon (58). Optical microscopy has been used to follow the growth of ZSM-5 from an amorphous gel under steaming conditions. Temperatures higher than 403 K were necessary for crystal formation, and surface dissolution of the gels preceded crystal formation (59).

Silicalite-1 has been synthesized from clear solutions of molar composition $25SiO_2/Na_2O/9TPAOH/450H_2O$ over a temperature range of 369–393 K (60). With increase in temperature, the length of induction time decreased from about 100 min at 369 K to about 14 min at 393 K. After the induction period, the mean diameter of the particles grew linearly with time. Growth rates ranging from 0.6 nm/min at 369 K to 3.7 nm/min at 393 K were observed. Measurements of particle number densities indicated a decrease of about two orders of magnitude over this temperature range: from 5×10^{11} at 369 K to about 2×10^9 at 393 K. At any given temperature, particle number densities remained essentially constant over the duration of the experiment.

For silicalite-1 formed from a reaction mixture of the composition $0.099TPABr/0.026Na_2O/SiO_2/24.8H_2O$ at temperatures of 423, 443, 458, and 473 (61), the length/width ratio of the silicalite crystals increased with temperature, as shown in Fig. 8, suggesting that the growth rate of different crystal faces varies with temperature (62). Direct measurements of rate of crystal growth for silicalite-1 has been reported at temperatures of 368, 393, 413, 433, and 448 K using the reaction composition $Na_2O/60SiO_2/3TPABr/1500H_2O/240EtOH$ (61). The aspect ratio (length/width) of the crystals increased with temperature, with the length growth rate having an activation energy of 80 ± 3 kJ/mol whereas the width growth rate had an activation energy of 62–81 kJ/mol.

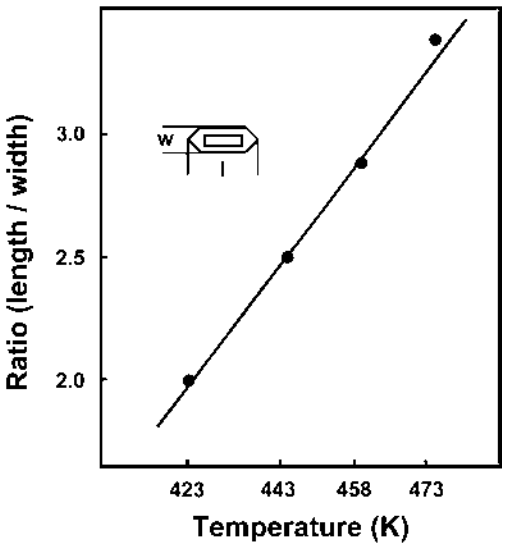

Fig. 8 The length-to-width ratio of silicalite crystals as a function of temperature, based on the average of 20 individual crystals at each synthesis temperature. (From Ref. 61.)

The synthesis of colloidal particle size silicalite-1 has been reported from clear solutions with molar composition: $9TPAOH/0.1Na_2O/25SiO_2/480H_2O/100EtOH$ at temperatures of 371, 367.5, 360.5, and 353 K (63). Although the linear growth rate increased with increasing temperature, the rate was more strongly dependent on the alkalinity of the initial composition than temperature, and a first-order surface reaction controlled growth mechanism with an apparent activation energy of 42 kJ/mol (63).

Growth at various temperatures led to the following conclusions:

The length of induction time decreases with increasing temperature, whereas crystallization rate increases.

Maximal crystallinity is reached in a shorter time at higher temperatures.

Fewer crystals are formed at higher temperatures.

The aspect ratio (*l*/*w*) increases with increasing temperatures.

C. Fluoride Medium

Fluoride ions play a similar mineralizing role as OH^- in alkaline conditions but typically results in larger crystals. Silicalite has been crystallized from compositions with variable fluoride and constant sodium content to study the influence of fluoride ions on crystallization. Crystallization from two series of gels having the general molar composition of xNaF-yNaCl-1.25TPABr-$10SiO_2$-$330H_2O$ (A) where $x + y = 10$ (x = 1, 2, 3, 7, 10) and xHF-yNaF-zNaCl-1.25TPABr-$10SiO_2$-$330H_2O$ (B) where $x + y = 10$ and $y + z = 10$ have been reported (64). Crystallization curves obtained from system A are shown in Fig. 9. These curves clearly indicate the enhancement of crystallization rate as a function of increasing fluoride content. Composition B showed that the crystallizing rate slowed on increasing HF in the medium. In agreement, another study also found a decrease in crystallization rate with increasing HF (64). Increasing HF did not decrease the pH of the medium substantially. The length of the crystals was used as a measure of the kinetics of crystal growth. It was found that the length increased with decreasing HF and increasing TPAOH. The aspect ratio also increased as a function of time. Chemical analysis showed levels of F^- of two ions per unit cell (64).

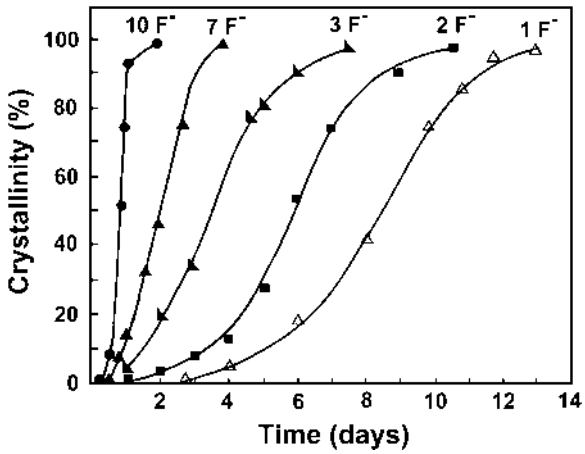

Fig. 9 Crystallization curves for the formation of silicalite at 443 K from gels of molar composition xNaF|yNaCl|1.25 TPABr|10 SiO_2|330 H_2O where x = 1, 2, 3, 7, 10 with $x + y = 10$. (From Ref. 64.)

The effect on crystallization of varying pH with constant Na^+, F^-, and TPA has been studied for the following compositions: *a*HF-*b*NaF-*c*NaCl-*d*TPABr-*e*TPAOH-10SiO_2-330H_2O with $a + b = 1$ (constant F^- content) and $d + e = 1.25$ (constant TPA content). For pH $\leq$ 2, no crystallization occurred (65). Comparisons of the crystallization results of silicalite OH^-- and F^--based systems provide interesting contrasts. Tavolaro et al. reported that the aspect ratio (length/width) for F^- systems was in the range of 2.8–5.0 and the crystal length growth rate was 0.17–2 μm/day (65). For high F^- content compositions, the activation energies for nucleation and crystallization have been reported as 10.8 and 9.1–10.6 kcal mol^{-1}, respectively (64). Comparable values reported for alkaline conditions were aspect ratios of 1–2.5, 1.8–2.7, and 0.9–9.4 depending on reactant composition. The growth rates for crystal lengths were 1.0–1.3 μm/h and crystal widths of 0.1–0.8 μm/h. The activation energies for nucleation and crystallization in alkaline medium were reported to be 4.8 and 10.1 kcal mol^{-1} (64). These data show that OH^- influences nucleation more than F^-.

The role of NH_4^+, Na^+, K^+, and Cs^+ cations in the synthesis of ZSM-5 in the presence of fluoride has been studied (66). The amounts of Al and alkali cations were varied in gels of initial composition 10SiO_2-*x*MF-*y*$Al(OH)_3$-1.25TPABr-330H_2O with M = NH_4^+, Na^+, K^+ and Cs^+; x = 9, 15, and 24; y = 0.16, 0.5, and 1.0. Potassium ion was found to be the most effective for incorporation of Al into the zeolite framework, while the ammonium-containing system was the least effective. The kinetic data showed that cations influence the reaction rates via electrostatic interactions and complex formation with fluoride anion in various siliceous and aluminosilicate complexes.

The crystallization of ZSM-5 from nonalkaline medium in the presence of fluoride ions occurred at the minimal F^-/Si ratio of 0.3 (67). The two organics used were tripropylamine (TRIP) and tetraethylammonium ion (TEA). Both ZSM-5 with a wide range of SiO_2/Al_2O_3 ratios and silicalite is formed with TRIP, but ZSM-5 could not be made with TEA when the SiO_2/Al_2O_3 ratio was greater than 400. The TRIP became protonated and trapped in the channels of ZSM-5. ZSM-5 has been synthesized in fluoride medium under dry conditions via a gas phase transport method, and SiF_4 was proposed to be the transport species (68).

Crystallization of silicalite in the presence of fluoride and competing templates has shown that TPA was entrapped in silicalite-1 whereas tetrabutylammouium occludes in silicalite-2 (69). ZSM-5 has been prepared in the Na_2O-SiO_2-Al_2O_3-$H_2N(CH_2)_6NH_2$-NH_4F system (70). The presence of F^- had significant influence on the nucleation and crystallization, and promoted the formation of ZSM-48. Silicalite-1 has been crystallized from a hydrothermal system containing silica and organics, such as propylammonium fluoride, choline cation diazabicyclo[2.2.2]octane, TPA^+, and F^- (53,71,72).

The influence of fluoride ions on synthesis can be summarized as follows:

- F^- plays the same mineralizing role as OH^-. Enhancement of F^- in the reaction composition leads to an increase in crystallization rate up to a certain level of F^-, beyond which a decrease is observed.
- The role of F^- is not mediated through influence on pH, though at a fixed F^- concentration, increase in pH increased the crystallization rate.

D. Mixed Solvent and Nonaqueous Systems

We discuss here crystallization reported with water-miscible solvents and organic vapors. The synthesis of ZSM-5 from gels containing silica, alumina, potassium and/or sodium hydroxide or chloride, diethanolamine (DEA), and water has been studied (73), with a typical gel composition being 2.6K_2O/1.2Na_2O/Al_2O_3/60SiO_2/32DEA/1200H_2O. A model based on the stabilizing effect of DEA via van der Waals forces for formation of theta-1 (pore filling) and ionic

interactions for formation of ZSM-5 (charge compensation) was proposed. The argument was advanced that the above roles for DEA extended to stabilization of nuclei (74). Crystallization of ZSM-5 in the presence of triethanolamine as a structure-directing and a mixed solvent system has been studied with varying Si/Al ratios (75). It was concluded that alkanolamines favor the crystallization of MFI structure only in the presence of Al (ZSM-5), but not in its absence, as tetralkylammonium salts do.

The synthesis of ZSM-5 has been reported in pure glycerol solvent system (76). Glycerol was found to act as both a solvent and a structure-directing agent. The crystallization was considered to progress by a liquid-phase ion transportation mechanism, in which the hydroxyl group of glycerol played an important role. Synthesis of silicalite-1 has been studied in the ethylene glycol solvent system using TPABr as a template (77).

The synthesis of diethylamine-silicalite-1 has been studied in a reaction mixture of diethylamine-NaOH-SiO_2-H_2O (54). The formation of diethylamine-silicalite-1 was favored by static conditions, high diethylamine concentrations, and low temperature (393 K). Diethylamine acted as a pore filler and solvent. ZSM-5 has been synthesized in ethylenediamine/triethylamine solvent system (78,79). Crystallization was found to strongly depend on the mole percent of triethylamine and SiO_2 and the molar ratio of Na_2O to triethylamine; a solid phase transformation was proposed for zeolite growth (78).

ZSM-5 zeolite has been synthesized using ethanol-water mixture as solvent (80). Dilution of the starting gel with water led to a decrease of both the nucleation and crystal growth rates, whereas the increase of ethanol/SiO_2 ratio favored both processes, indicating that ethanol was acting as a structure-directing agent.

ZSM-5 has also been synthesized in the vapor phase of ethylenediamine/triethylamine (81,82), propylamine/water, diethylamine/water, ethylenediamine/water (83–85), triethylamine/water (83,84), ethylenediamine/triethylamine/water, and 1-propanol/triethylamine (81) from amorphous aluminosilicate gels. The structure and crystallinity of the resultant zeolite depended on the composition of the organic vapor as well as that of the parent gel, with triethylamine and water promoting the crystallinity and ethylenediamine acting as a structure-directing agent.

ZSM-5 has been synthesized using seed crystals from acetone/water without any organic templates (86). A small amount of acetone in the reaction mixture inhibited the formation of quartz and facilitated rapid crystallization of ZSM-5 at 443–463 K, as shown in Fig. 10.

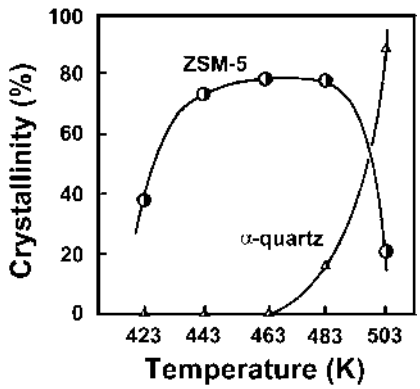

Fig. 10 Effect of synthesis temperature on the crystallization of ZSM-5 and α-quartz in 0.20 Na_2O|0.01 Al_2O_3|SiO_2|46 H_2O|1.3 acetone in a seeded system for 12 h. (From Ref. 86.)

Synthesis of ZSM-5 zeolite in the C_2H_5OH-Na_2O-Al_2O_3-SiO_2-H_2O system has also been reported (87).

From studies of mixed solvent and nonaqueous systems, the following conclusions can be drawn:

Alkanolamines as solvents can have a structure-directing role, and interaction with Al may play a key role in this process since they only structure-direct ZSM-5.

Alkylamines have been shown to have a pore-filling effect.

Addition of a solvent may help in suppressing competing phases.

Glycerol can act as a pure solvent in the absence of water, and the role of the OH groups in the glycerol for ion transport is proposed to be important.

Organic vapors can crystallize ZSM-5 from amorphous gel.

E. Seed Crystals

Crystallization in the presence of seed crystals provides important information regarding the growth mechanism and is also of practical value in speeding up synthesis.

The nucleation mechanism for an Al-free NH_4-ZSM-5 synthesis system has been examined by varying the size and mode of addition of the seed to the synthesis system (29). Enhanced nucleation and fast crystallization of new crystals were observed in contrast to the unseeded crystallization. Placing the seed crystals either at the top of the synthesis mixture or on the bottom of the autoclave or shaking the reaction mixture all had the same effect. However, crushing the seed crystals dramatically increased the nucleation rate, presumably due to the formation of very small crystalline fragments that served as nucleation sites.

The effect of amount of seed crystals has been studied (58). About 1–2% seed crystals was found sufficient for the complete crystallization of zeolite, and the crystallization period decreased. Further increase in the amount of seed crystals affected neither crystallization rate nor crystallite size. In presence of seed crystals, ZSM-5 was grown without a templating agent.

The stability of silicalite seeds has been shown to depend on the medium as well as the pretreatment (88). Calcined seeds dissolved in caustic solutions, whereas uncalcined seeds were more stable, presumably due to the stabilization by occluded TPA. Fresh seeds were shown to

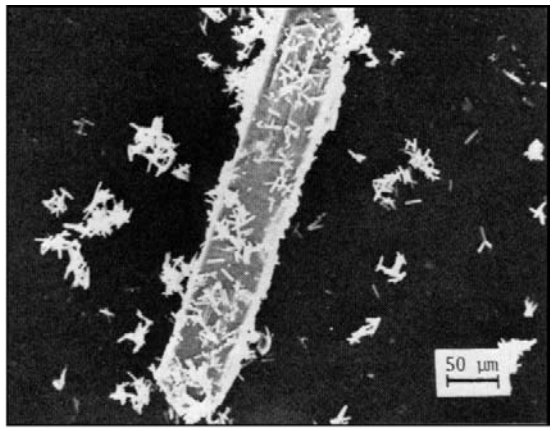

Fig. 11 SEM micrograph of a large 450 × 70 × 90 μm seed crystal exposed to 20 wt % seeds and showing the growth of numerous crystals on the seed. (From Ref. 89.)

grow in a silicalite synthesis mixture, whereas dried or calcined seeds grew but also produced a new population of nuclei that resulted from an initial breeding mechanism via microcrystalline dust on the seed crystals.

A series of studies were carried out with Al-free ZSM-5 seeds in order to investigate the effect of the presence of crystal surface (89). In spite of the relatively large amount of seed additions, very little growth of the seed crystal was observed, as shown in Fig. 11 for a synthesis with 20 wt % seed. Instead, new populations were observed to form around the seeds and on the seed surface.

The growth of silicalite in the presence of a very large seed crystal has been studied under a thermal gradient condition (90). The seed crystal was covered with specks of amorphous materials and randomly oriented silicalite crystals. The random orientation suggested that the newly deposited crystals were not epitaxially grown on the original seed surface. It was proposed that the new crystallites were formed by surface nucleation or by adsorption of nuclei from the solution. On sonication several rectangular "pits" were observed on the surface of the seed crystal, suggesting that the seed crystal was growing around the nucleated crystallites. If left in the growth environment for long periods of time, the seed crystals became covered with a polycrystalline mass of silicalite.

Crystal growth of silicalite and ZSM-5 in seeded systems has led to two proposed pathways of crystallization (91). Ordered growths and subsequently regular overgrowths were reported in sufficiently dilute synthesis mixtures. It was suggested that nucleation preferably took place on the seed crystal surface, and the seed crystal direction controlled the growth of new crystals, so that epitaxial growth was observed. In concentrated solutions, nucleation in solution dominated, and random formations of embedded crystals on seed surfaces were observed. It was proposed that initial breeding as a result of attrition from seed crystals was not important.

ZSM-5 was synthesized in ethanol and the effect of adding seed crystals on the growth process was studied (87). It was found that on increasing the seed amount, the rate of zeolite formation increased to a certain level and seeding only affected the initial nucleation period.

ZSM-5 has been crystallized from the organic free gel containing seed crystals (15).

ZSM-5 has been synthesized by using seed crystals from an acetone-water mixture system without any organic templates (86). A small amount of acetone in the reaction mixture inhibited formation of quartz.

Controlled nucleation and growth of ZSM-5 crystals has been achieved by using a semicontinuous reactor with or without seed crystals (92,93). Microwave zeolite synthesis is known to reduce the time of crystallization. It was found that the combined effect of nanocrystal seeding and microwave heating resulted in very rapid ZSM-5 crystallization, well before the reaction mixture reached the working temperature (94). The role of the microwave energy in energizing the seed surface and its environment was thought to be important in the accelerated growth.

Extensive studies of seeded growth have led to the following conclusions:

Seed crystals promote nucleation via the initial breeding nucleation mechanism due to the creation of small fragments that act as nucleation sites. Such nucleation is promoted by the use of crushed seed.

The history of seeds (fresh versus calcined) has important effects on crystallization.

Fresh seeds are shown to grow, whereas dried or calcined seeds grow but also produce a new population of nuclei that result from microcrystalline dust on the seed crystals.

Seed crystals usually lead to new populations of crystals rather than direct growth of the seed crystals themselves to become larger single crystals.

Seed crystals provide a route for crystal growth without the use of structure-directing agents.

The crystallization period decreases upon the addition of seed crystals, but only up to a certain number of seed crystals.

Seeding combined with microwave heating leads to very rapid crystal growth.

F. Solid-State Transformations

Solid-state transformation is possible within restricted conditions. A procedure for the pseudomorphic transformation of particles of silica gel to silicalite-1 has been described (95). One advantage of such methods is that the shape can be preserved. SEM showed that the particles were composed of large (~ 5 μm) loosely packed crystals surrounded by a dense crust of smaller (~ 1 μm) crystals.

Synthesis of ZSM-5 by water-organic vapor phase transport mechanism has been reported (96). The amorphous solids were first prepared, dried, and used for the vapor phase synthesis. This procedure demonstrated that solid hydrogel transformations in zeolite synthesis is possible (96). In another study, as long as the water content and the alkalinity of the powder were sufficient, the structure and crystallinity of the resulting zeolite depended on the composition of the organic vapor as well as that of the parent gel (79).

Dry aluminosilicate gels were transformed to MFI by a vapor phase transport (VPT) method using ethylenediamine (EDA), triethylamine (Et_3N), and water as vapor sources (82–84). The roles of water and amines in this crystallization were investigated. While Et_3N and water encouraged crystallization, EDA acted as a structure-directing agent. The support on which the dry gel was placed was found to be important. The product phase and purity as a function of the solvent mixture, precursor gel structure, and precursor gel chemistry has been discussed (84).

ZSM-5 has been crystallized from dehydrated amorphous gels (97,98). Autoclave was separated into two compartments by a sieve plate of pore diameter 0.6–1.5 μm. In one portion ZSM-35 was crystallized in liquid phase, whereas in the other portion ZSM-5 was crystallized as solid phase. The morphology of the ZSM-5 was found to be polycrystalline aggregates (97).

ZSM-5 has also been crystallized from a solid reaction mixture in fluoride medium starting with the reactant composition $(2.0–10.0)Na_2O/(30–800)SiO_2/Al_2O_3/(20–500)H_2N(CH_2)_6NH_2/(8–50)NH_4F$ (70). Increasing the amount of NH_4F in the reaction mixture enhanced the crystallization of ZSM-5. The same trend was observed for the wet synthesis mixture (64). The SiO_2/Al_2O_3 ratio has hardly any effect on the crystalline products in the system, whereas an optimal Na_2O/SiO_2 ratio (0.04–0.08) was found. It was difficult to synthesize zeolites under strong alkaline conditions in a solid reaction mixture.

Amorphous precursors obtained by drying aluminosilicate gels at 923 K were transformed into ZSM-5 in the presence of NH_4F and TPABr in the complete absence of solution phase (68). To explain zeolite formation, it was suggested that vapor phase transport of SiF_4 was taking place.

The solid-state transformation of kanemite into ZSM-5 in the presence of various Al sources has been reported (99).

Highlights of solid state transformation include the following:

Conversion of an amorphous material to a zeolite in the solid state is possible if transport of species can occur in the medium via vapor phase.

Use of fluoride reactants results in formation of volatile SiF_4 which acts as the mobile species.

Water can also be used for vapor phase transport.

III. NATURE OF CRYSTALS

In this section, we discuss the types of crystals that have been synthesized, some with considerable practical relevance.

A. Chemical Composition

Synthesis and spatial distribution of aluminum over ZSM-5 crystals has been systematically studied (100,101). From electron microprobe analysis of about ~50-μm crystals (100,101) it was inferred that the Al is primarily concentrated in the rim of the crystals (100). Althoff et al. (101) discovered that the extent of Al segregation depended on the synthesis conditions. Enrichment in the rim was found primarily in crystals with TPA, as shown in Fig. 12, whereas crystals made in the presence of 1,6-hexanediol or completely inorganic reaction compositions had homogeneous aluminum profiles (101). The rationale for the zoning in the presence of TPA was that TPA helped incorporate primarily silicate species, whereas for a Na^+ composition, aluminosilicate species were incorporated into the growing crystal (101).

Aluminum-rich ZSM-5 with Si/Al of 11 has been synthesized, corresponding to 8 Al atoms per unit cell (total of 96 Si, Al atoms). This is the lowest Si/Al ratio of ZSM-5 to date, and this limit is thought to be controlled by Al siting in only four-membered rings, as well as the number of charge-compensating cations in the narrow pore system. However, the mineral mutinaite has a Si/Al ratio of 7.6, indicating that nonconventional approaches may be required for crossing the barrier of 11 (102).

Relevant conclusions are as follows:

Al distribution within a crystal can be nonuniform and is controlled by reactant composition.

There is a lower limit of Al incorporation of Si/Al = 11.

B. Nanocrystals

The synthesis of discrete colloidal particles of TPA-silicalite-1 with an average particle size of less than 100 nm and with a narrow particle size distribution from clear homogeneous solutions has been reported (103). High alkalinities favored smaller crystallites, though the linear growth

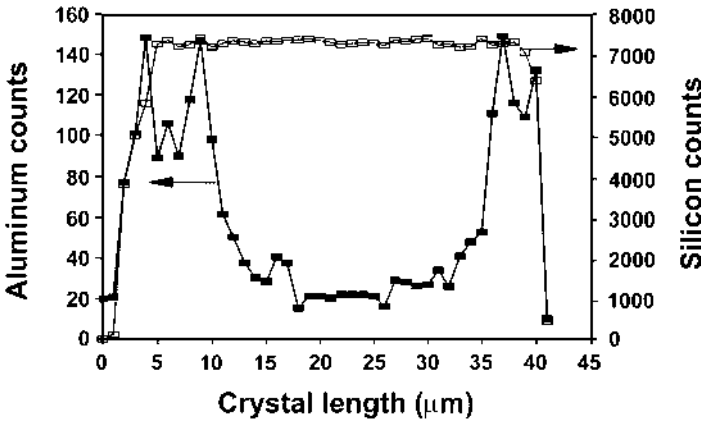

Fig. 12 Aluminum and silicon profile of a crystal from a TPABr-based synthesis with aluminum triethylate. (From Ref. 101.)

rates were not affected. Monodispersity was better with tetraethoxysilane over a polymeric source, such as silica sol (103).

Synthesis of colloidal ZSM-5 from clear homogeneous solutions was possible from synthesis mixtures with low sodium and high TPAOH concentrations (104). The size of the crystals was in the range 130–230 nm with a narrow particle size distribution. With increasing alumina concentrations, the crystal growth rate, the number of crystals produced, and the ZSM-5 yield decreased. The number of crystals produced decreased with increased alkalinity opposite to what was found for colloidal TPA-silicalite-1. Increasing alumina concentration was found to decrease the crystal growth rate, the number of crystals produced, the yield and size of ZSM-5 nanocrystals.

Nanocrystalline ZSM-5 (crystal size in the range 10–100 nm) has been synthesized from clear supersaturated homogeneous solutions in 24 h. The growth process was proposed to involve formation of an initial amorphous solid, which gradually transformed into nanocrystalline ZSM-5 through solid-solid transformations. In addition, the conventional formation of ZSM-5 from nuclei generated in the remaining liquid solution was observed after 48 h (105).

Confined space synthesis, a novel method in zeolite synthesis, has been used to synthesize nanosized zeolite ZSM-5 crystals with a controlled crystal size distribution (106).

C. Single Crystals

Synthesis of single crystals has made it possible to do detailed structural studies of MFI framework. Several synthetic procedures have been reported.

The hydrothermal growth of large monocrystals of TPA-ZSM-5 zeolite up to 420 μm has been reported. The samples consisted of fully crystalline and pure zeolitic phases with good homogeneity of the crystal sizes (107).

Single crystals of ZSM-5 were synthesized in systems containing Na^+-TPA, Li^+-TPA, and NH_4^+-TPA, respectively. Applying a reaction mixture of the molar composition 8TPA/$123(NH_4)_2O/Al_2O_3/59SiO_2/2280H_2O$, alkaline-free, homogeneous, and pure single crystals of ZSM-5 were prepared up to lengths of 350 μm (23). The crystal sizes and yields were found to be dependent on the water content of the starting reaction mixture and on the type of aluminum source.

Large single crystals of silicalite-1 has been synthesized with choline cation, 1,4-diazabicyclo[2.2.2]octane, and tetramethylammonium cations from nonalkaline medium (71).

Large crystals have made it possible to do detailed crystallographic studies. The framework of ZSM-5 belongs to the orthorhombic space group Pnma with cell parameters a = 20.07, b = 19.92, and c = 13.42 Å. Upon certain treatments, such as calcination and ion exchange, a displacive transformation (no bond breaking) to a monoclinic form has been noted (108,109). The orthorhombic-monoclinic transformation took place for high Si/Al ratio samples, while the orthorhombic symmetry was retained for dry air calcined samples characterized by low Si/Al ratios (110). X-ray photographs of single crystals of zeolite H-ZSM-5 at different temperatures have been presented (111). The reversible orthorhombic/monoclinic transition, previously observed with XRD and ^{29}Si MAS NMR on powder samples of H-ZSM-5, was noted. Ultrahigh-resolution ^{29}Si NMR has also been used to probe lattice changes with temperature changes or sorbents (112).

The location of TPA in the channels of a structure that is a precursor to fluoride silicalite was examined by single crystal XRD. The TPA was found to have the same geometry as in TPABr, with the N atom displaced from the center of the straight channel since the zig-zag and straight channels do not meet at the tetrahedral angle. The distance between the end C atoms of

adjacent propyl groups were found to be 2.7–3.1 Å, indicating that there was insufficient room for the replacement of propyl by *n*-butyl groups (72).

There has been some controversy about the exact geometry of the TPA ion in the zeolite. Chao and coworkers noted that there was a mirror plane symmetry, with $N(C_3H_7)_2$ part on the mirror plane and one C_3H_7 off the plane (9). van Koningsveld noted that the propyl-*N*-propyl fragments pointing in the sinusoidal and straight channels both have CNCC torsion angles of about 60° (113).

Crystals of ZSM-5 with Si/Al = 23 has been synthesized by an extended Charnell's method with sizes over 200 μm, and the space group of the crystal was found to be $Pn2_1a$ (R = 7.2%). It was suggested that there were three possible positions of Al (T(1), T(15), and T(18)) in 24 independent T sites, with the T(1) site most probable (114).

Relevant conclusions for this section are as follows:

In an alkaline-free system, homogeneous and pure single crystals of ZSM-5 are prepared up to a length of 350 μm. The crystal size and yield are found to depend on the water content of the starting reaction mixture and on the type of aluminum source.

There has been some disagreement as to the geometry of the TPA cation in the channel intersections.

The crystallographic orthorhombic-monoclinic transformation takes place for high Si/Al ratio samples, while the orthorhombic symmetry is retained for dry air calcined samples characterized by low Si/Al ratios.

D. Intergrowths

The systematic intergrowths (penetrating twins) observed with ZSM-5 crystals has been examined with transmission (TEM) and scanning (SEM) electron microscopy (115). The common feature was that adjoining crystals were rotated by 90° around a common *c* axis. It was proposed that this intergrowth nucleated from small areas on (010) faces of growing crystals. On (100) faces of large crystals, ramps were also observed in association with impurities.

Optical investigations of the intergrowth effects in the zeolite ZSM-5/ZSM-8 have been reported (116).

ZSM-5, ZSM-11, and ZSM-5/ZSM-11 intergrowths were synthesized from the same starting reaction mixture: $4.5(TBA)_2O\text{-}14.7M_2O\text{-}Al_2O_3\text{-}173.4SiO_2\text{-}24552H_2O\text{-}9Br$ where M = Na and/or K (117). X-ray powder diffraction and selection area electron diffraction were used to identify the intergrowth structures.

E. Membranes and Thin Films

Current applications of zeolites have driven the search for development of methodology for zeolite layers and films on various substrates. Layers are defined as a discontinuous assembly of crystals on a surface, whereas films are continuous dense phases. Films synthesized on a porous substrate are considered as membranes (118). Synthesis and applications of molecular sieve layers and membranes have been reviewed (118). ZSM-5 films have been prepared from clear aqueous solutions of synthesis mixtures with a high H_2O/SiO_2 ratio (119). Differences in morphology between outer and inner sides of the films have been noted. The outer side of the film was formed of an aggregate of crystals. Parts of the plane of the zeolite film were flat, indicating that some parts of the film strongly adhered to the wall of the Teflon sleeve. On the other hand, the clear shape of zeolite crystals was not observed in the inner side of the film.

The growth process of a ZSM-5 zeolite film was studied using EDX-SEM, TEM, and EDX-STEM. It was proposed that the ZSM-5 zeolite film was formed through a successive accumulation of zeolite crystals of 5–10 μm (120).

Silicalite-1 film formation on both untreated and plastically deformed copper substrates showed that film growth kinetics and morphology depended on the surface properties of the support (121). Film of silicalite-1 on steel and copper substrates have been reported (122). The film adhesivity, thermal stability, and morphology of the zeolite film were studied.

Films of ZSM-5 have been synthesized on a variety of flat nonporous surfaces including Teflon, silver, and stainless steel and on the external surface of porous Vycor disk (123). The side facing the support (Teflon) consisted of loosely held submicrometer-sized crystals, whereas the side facing the solution consisted of densely intergrown (twinned) crystals, 10–100 μm in size. Permeability studies with bicomponent gas mixtures showed that the membrane could discriminate between permeates at the molecular level because of the ZSM-5 pore system (123).

Self-supporting polycrystalline film of ZSM-5 with high crystallinity and adsorption capacities and one crystal thick, has been synthesized on polymer substrates (124).

There are several reports of films that proceed through a seeding step with colloidal seeds, followed by secondary growth (125–129). Carbon fibers were surface modified to promote adsorption of colloidal seed crystals of silicalite-1. Such particles were then adsorbed as a monolayer on the fiber surface and induced to grow into a continuous film of intergrown crystals of silicalite-1. Finally, the carbon fiber was removed by calcination in air, yielding hollow fibers of silicalite-1 (125).

Thin continuous films of ZSM-5 were formed on quartz substrates, starting with a monolayer of colloidal silicalite-1 seed crystals, which were grown into films with thickness of 230–3500 nm by hydrothermal treatment in a synthesis gel free from organic templates. The initial orientation of the crystals was with the *c* axis close to parallel to the substrate surface. During crystallization, the orientation changed to one with most of the crystals having the *c* axes directed approximately 35° from perpendicular to the substrate surface (126).

In another study, thin films of *c*-oriented ([00*l*]) and [*h*0*h*]-oriented silicalite films were grown by secondary growth process (127). It was possible to grow the columnar microstructure by repeated growth, leading to oriented films with thickness exceeding the wavelength of light and thereby optically transparent.

MFI films grown on silicon and quartz using silicalite seed led to thin films oriented with the *b* axes close to perpendicular to the substrate surface. In thick films, the *a* or *c* axes were close to perpendicular to the substrate surface depending on the conditions used for hydrothermal treatment (128).

A layer-by-layer self-assembly technique has been employed for the preparation of zeolite coatings on negatively charged polystyrene beads (129). The beads needed to be surface modified to facilitate adsorption of zeolite nanocrystals, prior to secondary growth.

Synthesis of zeolitic membranes is a very active area of research. We can conclude that:

Films can be grown on almost any support.

Seeded growth has opened new vistas for making zeolitic membranes.

IV. MORPHOLOGY

There has been considerable work on understanding those features that control morphology, since it reflects on the growth mechanism and is also of practical interest.

A. Dependence on Alkali Metal Cations

The morphology of ZSM-5 was found to be dependent on alkali ions (27). Li and Na zeolites consisted of spheroidal 2 to 5 μm and 8 to 15 μm crystal aggregates of very small platelet-like

units, respectively. A secondary nucleation process yielding smaller crystallites that deposit on the primarily formed larger crystals would explain the morphology. (NH_4)ZSM-5 consisted of large lath-shaped, well-developed, and double-terminated single crystals. The K, Rb, and Cs zeolites consisted of twins of rounded (K, Rb) or sharp-edged crystals (Cs), and the average size increased in the order Cs < Rb < K.

The (Li, Na)-, Na-, and (Na,K)ZSM-5 zeolites have been prepared at 443 K from highly dense gels of compositions $aM_2O\ bAl_2O_3\ 150SiO_2\ 490H_2O$ with M = Li, Na, or K; $0.9 \leq a \leq 8.82$ and $1.66 \leq b \leq 15$ (22). The morphology of the crystals were spherical or egg-shaped polycrystallites. Similar morphology of the ZSM-5 zeolites for Na and K have been observed (18). But in the bicationic system of Na, K, a morphology intermediate between those of Na and K zeolites was observed (18–20).

Morphology of ZSM-5 synthesized from Na-TPA, K-TPA, and Na,K-TPA depended on the alkali metal cation, TPA, and their ratio (19,20). For Na-ZSM-5, spherical agglomerate crystals smaller than 0.5 μm are observed. With both Na and K cations present at a ratio of K/(K + Na) = 0.75, large crystal aggregates were obtained. The morphology of the crystals grown from the K-TPA batch resembled those of intergrown disks, with sizes in the range 5–10 μm. When about 25% of the TPA was replaced with TBA, the aggregates were about 1.5 μm larger than those obtained using TPA alone. Synthesis of zeolite TPA-ZSM-5 with $(NH_4)_2O/Al_2O_3$ = 38 and different amounts of Li_2O, Na_2O, or K_2O has been studied (28). Addition of Li_2O produces unusually uniform, large, lath-shaped crystals of ZSM-5 $\sim 140 \pm 10$ μm in length.

Striking changes in morphology were obtained by the addition of NaCl, Na_2CO_3, and KCl salts. Single crystals and crystal aggregates in the fluidized size range, as well as completely crystallized aggregates in the fixed-bed ranges, changing in size from 100 to 200 μm were formed (19).

Considerable differences in morphology of crystals have been observed as a function of composition and synthesis conditions. The results can be summarized for inorganic systems as follows:

Different alkali metal cations result in distinct morphologies.

A mixed cationic system NH_4^+-Li^+ has been reported to form uniform, large, lath-shaped crystals of $\sim 140 \pm 10$ μm in length. NH_4^+ appears to direct formation of larger crystals.

Addition of salts can increase crystal size.

B. Dependence on Organic Cations

Lath-shaped crystals of ZSM-5 were obtained with tetrabutylammonium bromide (TBA), tetrapentylammonium bromide (TPeA), tributylpentylammonium bromide (TrBPeA), and tributylheptylammonium bromide (TrBHpA) (52).

The morphological changes for MFI-type zeolites with dipropylamine, tripropylamine, and TPABr has been reported (53). The TPA-containing crystals were elongated, whereas the crystals containing Pr_3NH and Pr_2NH were smaller with isomeric faces. Crystals were well shaped and elongated along the *c* axis for Pr to spheroidal shape for TPA and less and more aggregated structures for Dp and Tp, respectively.

The crystallization of ZSM-5 has been studied under controlled dosage of TPA (130). The TPA-free ZSM-5 crystals were elongated prisms whereas a controlled dose of 0.2 TPA/Al_2O_3 produces cauliflower-like coagulated balls (1–5 μm) of 0.05- to 0.2-μm crystallites. Other studies have been reported with Si/TPA ratios of 10, 24, and 48 (131). With a ratio of 10, tablet-shaped crystals formed with knobs on the top and bottom; for a ratio of 24, the crystals had a similar shape, with sharp corners and significantly larger. The larger size was a reflection

of lower TPA and reduced nucleation. With a Si/TPA ratio of 48, the size and shape remained the same as 24, but there appeared to be a solid phase growing on the surface of the crystals.

Starting with a composition of $12Na_2O/4.5(TPA)_2O/Al_2O_3/90SiO_2/2000H_2O$ which produces spherulitic aggregates of ~1 μm, a study was done to determine the effects of various additives to promote the growth of larger crystals (132). It was reported that partial to complete substitution of sodium salts for sodium hydroxide had a pronounced effect on resulting morphology, yielding crystals up to 80 μm, but with a wide range of sizes.

Silicalite-1 has been grown from reaction mixtures with varying TPABr content (133). All crystals were of a rod-like shape, and the volume of the individual crystallites was inversely proportional to the initial TPABr concentration, reflecting the fact that fewer nuclei are formed at lower TPABr concentrations. The aspect ratio of the crystals was similar for varying TPABr. Similar results were reported in which the alkalinity of the reaction mixture was varied over a range (134). The samples had almost monodisperse size distributions, and it was proposed that the growth occurred on the primary nuclei. The crystal size decreased as the alkalinity increased, indicating more nucleation, although at the highest alkalinities the yields were small. The highest aspect ratios were observed at lower alkalinities.

Crystallization kinetics and crystal morphology were determined for silicalites crystallized from two similar reaction batch mixtures (135). The batch compositions studied were $xNa_2O/8TPABr/100SiO_2/1000H_2O$ and $xTPA_2O/(8 - 2x)TPABr/100SiO_2/1000H_2O$, where x was varied from 0.5 to 4.0. As the alkalinity of the reaction mixture was reduced, the aspect ratio (length/width) of the crystals increased from 0.9 for $x = 4$ to 6.7 for $x = 0.5$. Both nucleation and crystallization occurred more rapidly in the presence of Na^+.

Synthesis of ZSM-5 in glycerol solvent has been reported and the morphology of the crystals found to be hexagonal columns (76).

Zeolite ZSM-5 has been synthesized in pyrrolidine-containing hydrous gels (136). The crystal habit is characterized by round-edged hexahedrons. Cubic crystals with uneven size and diameter ranging from 0.5 to 4 μm was obtained.

For compositions with organic cations, the following conclusions can be made:

Use of different structure-directing molecules changes the crystal morphology, as noted for the results with various amines.

Hydroxide ion content can alter morphology significantly.

Even for a particular ion, such as TPA, the amount used can alter the morphology. The crystallites tends to be larger at lower template concentrations, presumably because of formation of fewer nuclei. Similar effects have been noted with OH^- concentration.

Morphologies of crystals from mixed solvents or nonaqueous medium are distinct from comparable compositions in aqueous medium.

C. Dependence on Silica Source

NH_4-TPA-ZSM-5 system crystallized from two different silica sources produced different morphologies (30). From colloidal silica sol and TPABr relatively large (~35 μm) euhedral single crystals were obtained, whereas microfine precipitated silica and solution of TPAOH led to spherulitic aggregates of very small crystals.

D. Morphology of ZSM-5 in Absence of Organic Molecules

The morphological variation of ZSM-5 crystallized from template-free reaction mixtures have been compared with organic containing crystals (17). The crystal habit of the ZSM-5 crystals

synthesized in the absence of organics seems to be ellipsoidal as opposed to spheriodal, or cuboidal crystals using organic molecules.

E. Compositional Variation

On variation of composition (alkalinity, Si/Al ratio, TPABr), different morphologies were observed (137). Cubic crystals were obtained from highly alkaline media, and prismatic crystals from less alkaline solutions. The prismatic crystals were intergrowths and their surfaces defective. The cube-shaped crystals had side-on intergrowths, which upon magnification show smaller prismatic crystals. The crystal size increased on increasing the TPA/SiO_2 or Si/Al ratio (50,138). ZSM-5 synthesized by a rapid growth method produced more uniform size distribution (139).

Crystals of silicalite were well isolated whereas ZSM-5 with Si/Al of 25 contained polycrystals. It was suggested that at the high Si/Al ratios or in samples where no aluminum was present, a single nucleus was the source of each crystal, whereas for lower Si/Al ratios, a cluster of crystals grew from a multinuclei site (139).

The evolution of crystal growth morphologies has been explored using a Monte Carlo model. The model combined diffusive transport in the nutrient with thermally activated and local configuration–dependent steps for attachment, surface diffusion, and detachment (140).

V. GROWTH MODELS

Thompson and coworkers have pioneered various strategies to model zeolite synthesis (141). We briefly summarize these models followed by applications to the ZSM-5 system. Table 2 summarizes the important aspects of the different models.

A. Empirical Models

These models use mathematical relationships to fit the crystal growth data and lack the chemical fundamentals. For example, an exponential form such as $Z = Z_0 e^{kt}$, where Z_0 is the initial amount of the zeolite and k is a rate parameter, does describes the data at early times but does not provide much insight into the process. There is no suggestion of nucleation; both nucleation and growth are treated by the same rate parameter and the process has no termination.

Other empirical models have considered the nucleation rate to be the inverse of induction time (time during which crystals are absent) and crystal growth rate as the slope at the midpoint of the crystallization curve. Based on such data for ZSM-35, it was shown that the nucleation rate has a $[OH]^{2.5}$ dependence, whereas the crystal growth rate has a $[OH]^2$ dependence. Such models have been criticized because they imply that nucleation proceeds at a constant rate during induction, stops immediately upon crystal growth, and is followed by a constant growth rate. Such a process is an oversimplification of zeolite crystallization.

B. Reaction Engineering Models

In this approach, three components are considered: gel (G), dissolved gel (G*), and zeolite crystals (Z). The reactions involved are as follows:

$$\mathrm{G} \xrightarrow{k_1} \mathrm{G}^*$$

$$\mathrm{G}^* + \mathrm{G} \xrightarrow{k_2} 2\mathrm{G}$$

$$\mathrm{G}^* + \mathrm{Z} \xrightarrow{k_3} 2\mathrm{Z}$$

Table 2 Salient Features of Zeolite Growth Models

Model type	Key features
Empirical	Not based on fundamental theory Not predictive Arbitrary constants Constants not true constants, but lumped parameters
Reaction engineering	Phases treated as elements No consideration of particle size distribution Semipredictive capability Easy to solve: (a) batch reactor—ordinary differential equations (b) CSTR—algebraic equations
Population balance models	Based on fundamental theory Particle size distribution assumed Much more information predicted Predictive capability More effort to solve: (a) Batch reactor—partial differential equations (b) CSTR—ordinary differential equations
Avrami model	Developed for solidification of metals, assumes a population of germ nuclei, separates nucleation and crystallization Predicts end of crystal growth Complete model not applied to zeolite synthesis
Pseudocell model	Uses a fraction of unit cell as pseudocell as monomer, transfer of pseudocell between phases Parallels polymerization concept where pseudocells combine to form oligomers Uses population balance model as mathematical framework

Source: Ref. 141.

where k's are rate constants. Using the quasi-steady-state assumption for G* results in a rate expression:

$$\frac{dy}{dt} = a_2[\mathrm{OH}]^{a_1}\frac{y(1-y)}{\mathrm{a}_3 + (1-y)}$$

where y is the percent conversion of reagent and a's are constants. Here, the zeolite is produced autocatalytically, implying the presence of zeolite at time $t = 0$. Novella et al. included a nucleation step

$$\mathrm{G} \xrightarrow{k_4} \mathrm{Z}$$

and derived

$$\frac{dy}{dt} = K[\mathrm{OH}^-]^{x_1} \quad (1-y)y + k_4 y$$

where K is lumped constant and x_1 is percent crystallinity of solid. The problems with the reaction engineering models include the empirical dependence on $[\mathrm{OH}^-]$ and the fact that no information is obtained regarding crystal size distribution.

C. Population Balance Models

The population balance model has enjoyed considerable popularity for zeolite crystallization since it can predict crystal size distributions. It is based on conservation of particles growing along a size axis and takes the form

$$\frac{\partial n}{\partial t} + Q\frac{\partial n}{\partial L} = 0$$

where $n(L, t)$ is the crystal size distribution and Q is the crystal growth rate. Applying the moment transformation to the above equation results in ordinary differential equations that can be solved to provide number, length, area, and volume of crystals. For a cubic geometry, the third moment (volume of crystals, V) takes the form

$$V_c = \frac{BQ^3}{4}t^4$$

where B is the nucleation rate and V_c is the volume for cubic crystals. This equation was used by Zhdanov to analyze zeolite crystallization data at small times. Because B and Q were constant and unconstrained with time, unbound growth with time is predicted. Various studies have been reported where B and Q are time-dependent functions, are chosen empirically, and provide better fits with the experimental data. The analytical result of the population balance model usually results in a polynomial dependence of crystallinity on time. Seeded systems can be adapted to the population balance model by setting the nucleation rate B to 0.

D. Avrami Model

The basis of the Avrami model is that there are $\bar{N}$ germ nuclei present at $t = 0$, which grow; therefore, $\bar{N}$ decreases with time until all of the nuclei have grown ($t = \bar{\tau}$). After this time, only crystal growth continues. For $\tau < \bar{\tau}$, the volume fraction of the new phase takes the form:

$$V\tau = 1 - e\frac{-\beta\tau^4}{4!}$$

and for $\tau < \bar{\tau}$:

$$V(\tau) = 1 - e^{\beta|E_3(-\tau) - e^{-\bar{\tau}}E_3(\bar{\tau}-\tau)|}$$

$$\text{where } \beta = \frac{6\sigma Q^3\overline{N}}{B^3}(\text{constant})$$

$$\text{and } E_3(-\tau) = e^{-\tau} - 1 + \tau - \frac{\tau^2}{2!} + \frac{\tau^3}{3!},$$

For small τ

$$V(t) = \frac{\sigma BQ^3\overline{N}}{4}t^4$$

and has the same form as the population balance model.

E. Pseudocell Model

This model is an extension of the reaction engineering model, in which conservation of pseudocells (a fraction of a unit cell of a zeolite) in each phase is maintained and rate constants for transfer of pseudocells between phases are used to fit the experimental data. The nucleation process is represented by the combination of two pseudocells, whereas crystal growth is considered the addition of a single cell to the crystal surface. The pseudocell model has been incorporated into the population balance model using a classical homogeneous nucleation rate and a size dependent linear crystal growth rate. Results from this simulation for zeolite A are shown in

Fig. 13, where the nucleation rate (B), average crystal size (L), percent crystallinity (R), and relative concentration of unit cells (G^*/G_0) in the liquid medium are shown as functions of time (141).

With this brief background, we focus on the applications of these models and their limitations. Population balance models have shown a discrepancy between predicted crystallinity and the observed crystallization during the early stages of growth, i.e., during the induction period. Thompson and coworkers noted that introduction of a lag time prior to beginning of nucleation and crystal growth led to a decrease of q (percent crystallinity $\propto t^q$), but still overestimated q from its theoretical value of 4. In that study, they also demonstrated that the phenomenon of size-dependent solubility (Kelvin effect) is not responsible for the lag time (142).

Crystallization data for ZSM-5 were used to suggest that nucleation of the zeolite occurred by both heterogeneous and autocatalytic mechanisms. Heterogeneous nucleation occurred at the gel–liquid boundary and on impurity sites in the liquid phase. The nuclei in the inner pockets of the gel were released into the liquid phase and provided an accelerating impetus to the zeolite crystallization via the autocatalytic route. A fit of the experimental data is shown in Fig. 14, which shows the crystallinity of ZSM-5 as a function of time for the composition $5Na_2O/8.8(TPA)_2O/0.626Al_3O_3/100SiO_2/1250H_2O$. The equation used to fit the data was $Z(t) = K_{ht}t^3/(1 - K_at^3)$, where K_{ht} represents the kinetic constant for nucleation at the solid–liquid interface and K_a represents the autocatalytic nucleation process (143). The crystallization rate, as determined by the zeolite fraction as a function of time, agreed well with the model. The nucleation rate was found experimentally to peak in the early part of crystallization.

However, using the same parameters used in Ref. (143) for fitting the crystallization curve, Thompson noted that the predicted nucleation occurred much later than what was

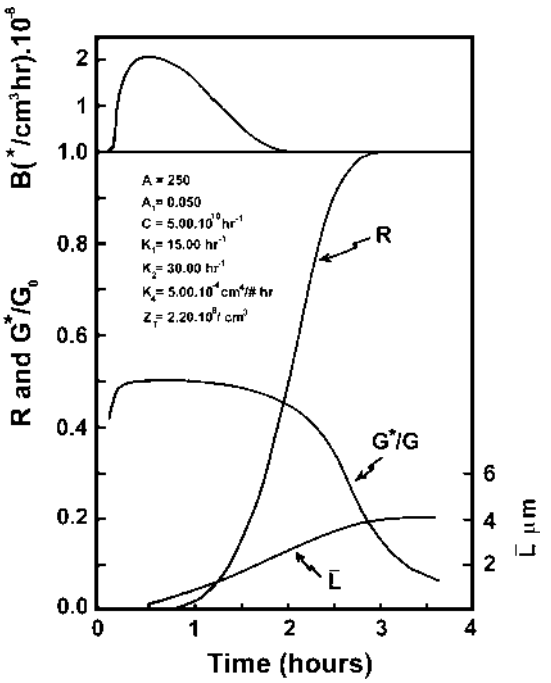

Fig. 13 Simulation of zeolite synthesis from modified population balance model for batch synthesis of zeolite A, with nucleation rate (B), crystal size (L), percent crystallinity (R), and relative fluid phase concentration of unit cells (G^*/G_0) as a function of time. (From Ref. 141.)

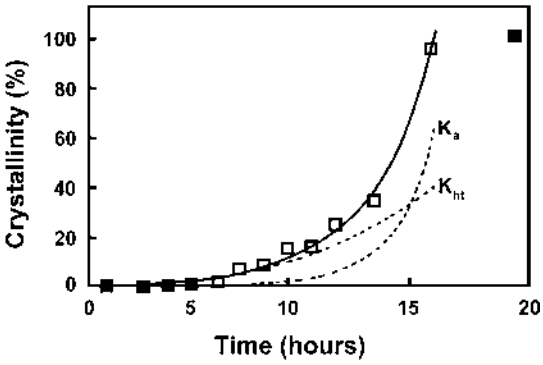

Fig. 14 Best-fit curve of crystallization kinetics for a ZSM-5 composition (solid line). Dashed lines show the contribution from heteronuclei (K_{ht}) and nuclei released by dissolving gel (K_a) to the crystal growth process. (From Ref. 143.)

experimentally observed, suggesting that there may be some heterogeneity in distribution of the nuclei in the gel and that the autocatalytic nucleation needed further examination (144).

A model that adjusted the autocatalytic nucleation hypothesis by suggesting that nuclei were located preferentially on the outer surfaces of the gel provided a better fit of the nucleation rate values, crystallization curves, and crystal size growth for ZSM-5 (145).

Aging of the amorphous gel at low temperature followed by elevated temperature crystallization was simulated by population balance methods (146). The aging step resulted in the formation of viable nuclei that effectively lay dormant until the temperature was raised. Increased aging led to smaller induction times and faster crystal growth. The simulation also predicted smaller final average crystal size with aging (146).

The method of chronomal analyses (dimensionless time analysis) according to Neilsen has been applied to the growth of discrete colloidal particles (particle sizes of less than 100 nm) of TPA-silicalite-1 to gain information on the crystal growth mechanism (63).

Modeling of zeolite growth has led to insight into the crystallization process, though an exact mathematical description of the process is still lacking.

Use of models that employ a constant supersaturation as initial condition leads to an overprediction of crystallization rate, suggesting the important role of solution-based transformation to produce the relevant species.

Avrami transformation kinetic studies suggest that nucleation and growth stage of the crystallization process needs to be separated.

Population balance models have been used with success in predicting batch zeolite crystallization behavior based on homogeneous nucleation.

Heterogeneous and autocatalytic nucleation models have also been developed, although use of the latter has been controversial.

For gel-based synthesis, population balance models suggest that the aging step involves formation of nuclei, whose number rather than size is the critical parameter in determining crystallization dynamics.

VI. CRYSTAL GROWTH PROCESSES

We conclude this chapter with a discussion of the pathways through which crystallization can proceed. We begin with the global features associated with the synthesis, followed by a more molecular level description of the growth process.

A. Fundamentals of the Crystallization Pathways

Several studies support the idea of solution-based crystal growth. Based on elemental analysis, NMR and surface spectroscopy of various phases present during crystallization of ZSM-5, a nucleation process that begins at the gel–liquid interface, and crystal growth via liquid phase transportation was proposed (24). Dissolution and complexometric analysis of a dilute Na,TPA-ZSM-5 system has been interpreted as conversion of the amorphous precursor material into a crystalline product via a solution-mediated process, with the concentration of dissolved silica species remaining relatively constant. The zoned composition of the Na-TPA-ZSM-5 crystal product was shown to be a natural consequence of the composition during the synthesis (147). Though the role of particular silicate species was not determined, it was proposed that all solution species may contribute to some extent, with possibly the monomeric species being most important (147). It has been suggested that for ZSM-5 formation a silicalite-like zeolite initially crystallizes followed by aluminum entering the framework through dissolution of the crystal aggregates (148). For MFI-type zeolites synthesized by the rapid crystallization method in 2 h, the pH of the initial hydrogel was found to be the most critical parameter (139). The change in pH for synthesis of high-silica zeolites from gels was correlated with solubility of the gel and crystals (149). The model predicted that for a given concentration of quaternary ammonium ions, the highest increases in pH were associated with the most stable zeolite, whereas a lower pH change was associated with an unstable zeolite or amorphous phase.

The microstructural evolution in the nucleation stage of a synthesis reaction of ZSM-5 zeolite has been studied, with particular emphasis on the role of the organic cation, TPA (150). Direct observation of the microstructure has been achieved by cryotransmission electron microscopy.

Several techniques exist for observation of *in situ* growth of crystals. *In situ* crystal growth of ZSM-5 crystals was observed using optical reflection microscopy (59,151) of amorphous gel and clear solutions. In the case of ZSM-5 formation from gels, it was reported that after the induction time certain crystals grew to 10–20 μm, after which no further growth was observed. On the other hand, in the case of silicalite crystals from clear solution, the induction time was not observed. Based on Fig. 15, the growth rates of the silicalite crystals were determined to the 0.35 and 0.1 μm/h for length and width, respectively. The activation energies of silicalite were calculated to be 52 and 28 kJ/mol for growth along length and width, respectively (151). Previous values reported were 64.5 and 46.5kJ/mol (61). For, ZSM-5, the activation energy has been reported as 80 kJ/mol (62).

Dynamic and static light scattering techniques have been used for the direct *in situ* observation of a crystallizing silicalite system (60). An initial "induction time" existed during which the initial germ or nonviable nuclei were generated from the silicate species and grew to a critical size before spontaneous crystal growth. After the induction time, the particles grew linearly. By filtering off the product after 100-nm particles were formed and then returning the filtrate to hot stage, it was shown that new particles nucleated indicating that nucleation is a continuous process. Both growth and nucleation rates were shown to be considerably enhanced by an increase in reaction temperature. The dilution had marginal effect on the growth but induction time increased. Increase in aging time increased the number of nuclei and growth rate.

In another study, the linear growth rate of silicalite particles at 373 K was determined by light scattering to 3.79 nm/h—a low value that was ascribed to the synthesis conditions employed. Furthermore, the particle number concentration was shown to be constant, indicating that no secondary nucleation event occurred during the growth process. The crystallization kinetics reported in the temperature interval 353–373 K correlated with a first-order surface

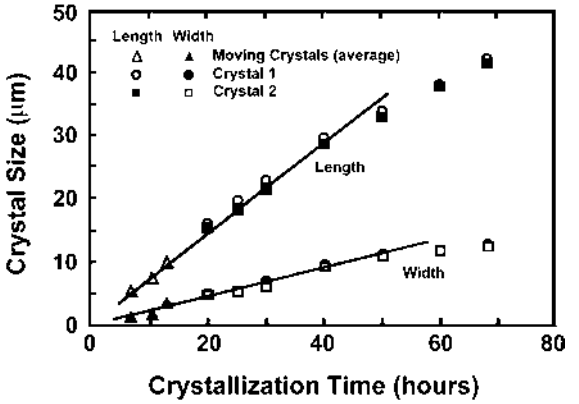

Fig. 15 Growth of stationary and aggregated moving silicalite crystals. Crystals 1 and 2 are stationary and exhibit linear growth of length and width over a long time range (up to 50 h). Aggregated moving crystals are smaller than stationary crystals, indicating the decline in growth rate due to exhaustion of chemical species around them. Crystallization temperature: 438 K (0 hour corresponded to the start of heating). (From Ref. 151.)

reaction controlled growth with an apparent energy of activation of 42 kJ/mol. A diffusional mechanism and a compound growth mechanism in which both surface reaction and diffusion compete for rate control were ruled out (63).

The method of Zhdanov and Smulevich was used to analyze the crystal growth rate and nucleation behavior of silicalite-1 (152). From data on reactions run under different conditions at 368 K, the linear growth rate ($0.5dl/dt$) was determined to be in the range $(1.9–2) \times 10^{-2}$ μm/h. However, the different reactions did not show the same pattern of crystal mass increase with time, the variations reflecting differences in nucleation behavior. All of the nucleation rate curves were either bimodal or trimodal, suggesting that at least two separate nucleation mechanisms were operating. Early in the reaction, nucleation was probably heterogeneous and associated with the amorphous gel or colloidal material present in the mixture. Later on, when appreciable quantities of crystalline product had formed, an additional crop of crystals nucleated either by a secondary mechanism or by release of further heteronuclei from the dissolving amorphous component. The results confirmed that simple growth curves based on XRD crystallinity were of limited use in understanding the complex processes occurring in zeolite synthesis.

In a controlled monolithic crystal growth in a semicontinuous reactor system, the effect of increasing nucleation rate has been studied (92,93). The initial result was a broadening of the crystal size distribution; at highly enhanced nucleation rates polycrystalline aggregates were obtained. The trends observed were rationalized in terms of (a) the rate of nutrient supply, (b) the crystal surface area available for mass deposition, and (c) the chemical limitations to growth at the crystal surface.

The following conclusions can be made from the above studies:

Based on powder diffraction and spectroscopic methods a typical kinetic curve includes an induction period during which germ/nonviable nuclei were generated, a transition period of slow growth, followed by rapid crystal growth. The curves have a sigmoid shape.

Compositional effects have a profound influence on the kinetics. Increased template concentration and dilution have opposing effects on crystal growth, with the former accelerating the kinetics.

For a given concentration of quaternary ammonium ions the highest increases in pH were associated with the most stable zeolite, and the yields depended primarily on the stoichiometry of the reaction mixture.

Modeling of a clear solution synthesis in which no secondary nucleation was present allowed the authors to extract growth rates, activation energies, and the exclusion of a diffusional and compound growth mechanism of crystallization.

Dynamic light scattering allowed for the monitoring of growth in particle size and clearly showed a nucleation followed by a growth phase. Nucleation would continue indefinitely if crystals were removed from the medium.

Increase in aging time increased the growth rate and number of growing nuclei in the system, which is the consequence of more germ nuclei present on increased aging that are active in further growth.

There is evidence that under certain compositional conditions there can be several nucleation events, either by secondary nucleation or by release of heteronuclei from the gel, showing the complexity of the process, which would not be obvious from diffraction or spectroscopic measurements.

Composition conditions that lead to enhanced nucleation result in polycrystalline aggregates controlled by nutrients, crystal area available for growth, and chemical limitations to growth at the crystal surface.

B. Nature of Intermediate Phases

A large number of studies have focused on the structure of the intermediate phases that exist prior to crystal formation.

Crystallization of ZSM-5 from pyrrolidine-Na_2O-Al_2O_3-SiO_2-H_2O has been investigated, and the suggestion that pyrrolidine stabilizes five-membered aluminosilicate rings was made (136).

Prior to detection of ZSM-5 by powder diffraction, infrared (IR) and catalytic properties of the amorphous phases were typical for ZSM-5 (153). Solid-state ^{13}C NMR spectroscopy has shown the conversion of amorphous material to crystals (154).

The XRD amorphous material, prior to crystal formation, consisted of an aluminum-rich phase. This was followed by TPA-ZSM-5 entities with dimensions of the order of the unit cell of ZSM-5, which eventually recombined to form the crystalline framework. The framework defects found in the XRD crystalline TPA-ZSM-5 by ^{29}Si magic angle spinning (MAS) NMR disappeared upon calcinations (154).

Raman spectroscopic study of the ZSM-5 has been reported (155,156). As shown in Fig. 16, TPA is found to be trapped in the amorphous gel at the earliest stages of the synthesis in an all-trans configuration. Upon crystal formation, there is a change in orientation of the TPA cation, suggesting that long-range crystalline order forces a conformational change in TPA to accommodate it within the channels.

IR spectroscopy has been used to identify the ZSM-5 zeolite (157).

ZSM-5 synthesized at a relatively low temperature (363 K) in atmospheric condition required a long induction time (158). During this induction time, samples were analyzed by XRD, IR, NMR, and SEM. It was reported that at the initial stages (after 5 h), there was the formation of amorphous lamellar particles. These thin and lamellar particles were fragile. As the crystallization proceeded, numerous bead aggregates were formed on the surface of the Si-rich intermediate particles and transformed into highly siliceous ZSM-5 crystals. It was proposed that the dissolved amorphous phase played the role of Al-rich source during the crystal growth.

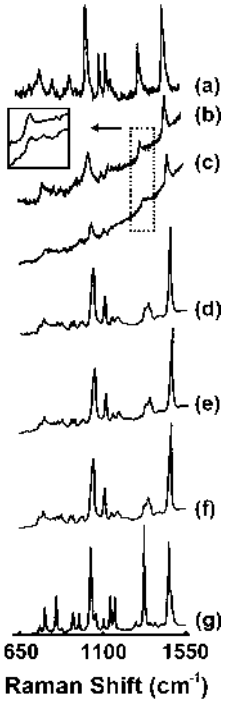

Fig. 16 Raman spectra in the region 650–1550 cm^{-1} of (a) 0.5 M tetrapropylammonium bromide, and solid samples present during various stages of zeolite crystallization; (b) 1 day; (c) 3 days; (d) 4 days; (e) 6 days; (f) 9 days; and (g) tetrapropylammonium bromide crystals. (From Ref. 155.)

Based on these studies, a mechanism of ZSM-5 crystallization was proposed. ^{29}Si NMR study of the liquid phase during the induction period found only the presence of Q^0 and Q^1 units, indicating their possible role in nucleation. However, the possibility that other species were immediately attached to the lamellar solid phase and hence unobservable in solution exists.

A crystallization scheme has been proposed based on small- and wide-angle X-ray scattering (SAXS-WAXS) (159). The results indicated that cluster aggregation occurred before crystallization. These aggregates were composed of primary particles, which may be hydrated TPA-silicate clusters. With time, the clusters densified into mass fractal aggregates and subsequently into surface fractal aggregates. The size of this structure increased very slightly with time, indicating that additional primary particles were transported from solution or other silica aggregates to the densifying cluster. The occurrence of crystalline structures was observed simultaneously with WAXS. Crystal growth occurred by combination of the densified primary aggregates into kinetically determined secondary aggregates, which subsequently densified into energetically more favorable, dense, smooth particles. The schematic representation of the crystal growth process is shown in Fig. 17. The interesting feature of the results is that also in the homogeneous system a precursor aggregate is being proposed before crystallization, similar to a gel reorganization mechanism of zeolite crystallization. Thus, in both homogeneous and heterogeneous crystallization an intermediate gel phase may be necessary before crystallization can occur.

The formation and consumption of precursors upon crystallization of Si-TPA-MFI using simultaneous, time-resolved, SAXS, WAXS, and USAXS found that crystal growth

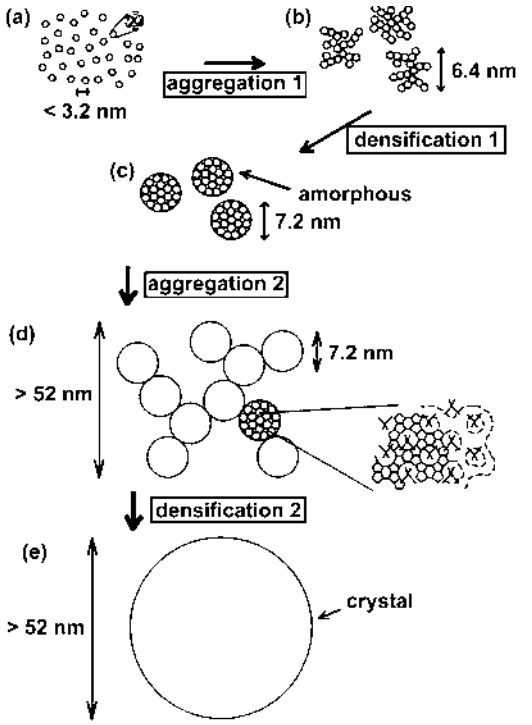

Fig. 17 Mechanism of microstructural random packing, subsequent ordering, and crystallization. (a) Silicate-TPA clusters in solution, (b) primary fractal aggregates formed from the silicate-TPA clusters, (c) densification of these primary fractal aggregates, (d) combination of the densified aggregates into a secondary fractal structure and crystallization, and (e) densification of the secondary aggregates and crystal growth. (From Ref. 159.)

process occurred by addition of 2.8-nm primary units onto the crystal surface, with an apparent activation energy of growth of 83 kJ/mol (160). In a similar study using the same techniques, the group concluded that the 2.8-nm particle aggregated to form 10-nm particles, which then went to form the viable nuclei that were responsible for growth of silicalite crystals (161).

Small-angle neutron scattering (SANS) has been used to study gels from synthesis of ZSM-5, and scattering length densities of the gel particles and their texture were determined using contrast variation methods. Gels formulated from soluble silicates incorporated TPA molecules promptly into an amorphous "embryonic" structure, and crystallization ensued via a solid hydrogel transformation mechanism. Gels formulated from colloidal silica showed different scattering behavior, and a liquid phase transport mechanism was inferred (162). This same group also used SAXS and SANS to propose a mechanism for silicalite crystallization from clear solution. The basic unit was estimated to be 8 nm in diameter and 14 nm in length with cylindrical features. Growth of these primary particles was proposed to occur along the cylinder axis by fusion. Units of diameter 8 nm and length of 33 nm were noted. It was suggested that these larger units had a well-organized MFI core, whereas the outer shell was defective. Crystal growth occurred by aggregation of the particles, in which surface reconstruction occurred upon fusion and resulted in crystal formation.

The SAXS-WAXS measurements, together with high flux of synchrotron radiation and a high-pressure reaction cell, were used to probe in situ the synthesis process and it was found that reorganization of the gel occurred before crystallization began (163).

The silica species present in an aged clear suspension, which upon heating formed silicalite-1, were extracted with 80% efficiency using a sequence of acidification, salting out, phase transfer into organic solvent, and freeze-drying methods (164). Based on X-ray scattering, TEM, atomic force microscopy, and ^{29}Si MAS NMR spectroscopy of these particles, they were proposed to be slab shaped, with dimensions of $1.3 \times 4.0 \times 4.0$ nm^3. These nanoslabs were found to be amorphous and proposed to have the MFI structure with nine channel intersections per particle, each containing a TPA cation. Additional studies by this group have focused on the silicate ions present in solution. Based on NMR and IR spectroscopy, it was proposed that the slabs were formed from species that included bicyclic pentamer, pentacyclic octamer, tetracyclic undecamer, and a trimer (Fig. 18). Fig. 19 shows a trimer species and its aggregation to form a nanoslab. These nanoslabs were proposed to have propyl groups sticking out on three sides and micropore openings on the opposite side form the holes. Under ambient conditions, the propyl groups cause repulsion between the nanoslabs; thus, higher temperatures are required to cause aggregation of the nanoslabs into crystals. A mechanism for aggregation of nanoslabs to form tablets and stacking of these tablets followed by their packing to form crystals has been proposed (165–167).

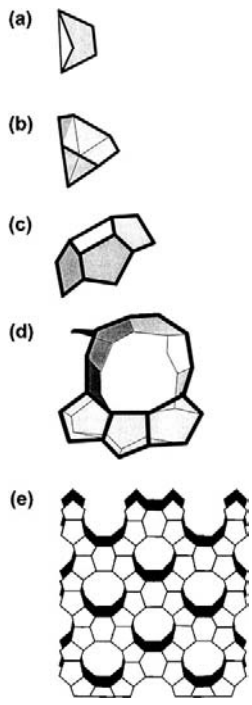

Fig. 18 Siliceous entities proposed to occur in the silicalite-1 crystallization from the TPAOH-TEOS system: (a) bicyclic pentamer, (b) pentacyclic octamer, (c) tetracyclic undecamer, (d) trimer, and (e) nanoslab. (From Ref. 165.)

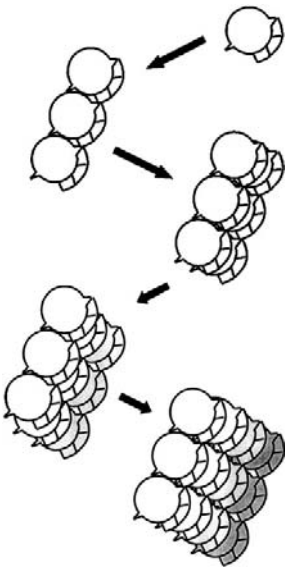

Fig. 19 Proposed mechanism of nanoslab formation by aggregation of trimers in the crystallization of silicalite from clear solutions. (From Ref. 165.)

Following conclusions can be made regarding the intermediate stages prior to crystal formation:

At the initial stage of nucleation, there is the formation of lamellar particles that are amorphous.

Even though crystallization originates from the homogeneous system, cluster aggregation occurs before crystallization starts in analogy to the heterogeneous system.

Crystal growth occurs by combination of the densified primary aggregates into kinetically determined secondary aggregates by combination of already growing nuclei, which subsequently densify into energetically more favorable, dense, smooth particles.

Specific structures of the primary aggregates have been proposed.

X-ray amorphous material exhibiting zeolite-like properties has been isolated, suggesting that domains of zeolite-like structures exist in the gel prior to crystal growth.

Several independent methods suggest the formation of intermediate "aggregated" structures at early stages of the crystallization process. These amorphous embryonic structures evolve to crystals by restructuring and incorporation of nutrients.

C. Molecular Precursors

There have been many attempts over the years to identify the molecular precursors essential to the formation of a specific framework.

Using ^{29}Si NMR spectroscopy and trimethylsilylation followed by gas chromatography, the occurrence of double-ring silicate anions was discovered in tetraalkylamonium hydroxide silicate solutions. The double-five-ring (D5R) silicates increased with decreasing OH^-/Si ratio and were even detected at 373 K during the crystallization of ZSM-5. It was hypothesized that these D5R silicates can be precursors for ZSM-5 (168). However, as pointed out by Knight, evidence for the above hypothesis is completely lacking and the idea of zeolite growth by sequential addition of secondary building units from solution needs to be "laid to rest" (169).

Siliceous synthesis gels containing tetraalkylammonium (TAA^+) and sodium cations were examined using X-ray diffraction, elemental analysis, ion exchange, ^{29}Si MAS NMR spectroscopy, and SEM (170). The TAA cations were encapsulated in silicate cages, and it was proposed that silicalite is formed via the rearrangement of these cages by the breaking and reformation of siloxane bonds. TBA because of its large size does not conform well to the silicalite lattice, thus forming an intergrowth of the silicalite-1 and silicalite-2 structures. TEA cations were encapsulated in silicalite cages, but not to the same extent as TPA and TBA, presumably because TEA is not as hydrophobic. No silicalite formed in the TEA silicate gel. The addition of TRIP to a TPA silicate gel had no effect on the kinetics of silicalite formation, since TRIP is neutral and no electrostatic attraction to the negatively charged surface of the gel was present.

The role of TPA as a structure-directing agent in the nucleation and crystallization of ZSM-5 has been studied by ^1H-^{29}Si CP MAS NMR technique (171,172). It was proposed that favorable van der Waals contacts between the alkyl chains of TPA and the hydrophobic silicate species resulted in an inorganic–organic composite, driven by entropy changes, and that these preformed inorganic–organic composite species were responsible for nuclei formation.

Another study of the interactions of the TPA cation with its surroundings in the early stages of the synthesis of a siliceous MFI zeolite gel by in situ ^1H, ^{14}N and ^{29}Si NMR spectroscopy found that hydrogen bonds between the organic and H_2O-clathrated molecules were progressively replaced by hydrophobic interactions between the organic and silicate species. This feature occurred in the solution phase of the gel and reduced the motion of TPA. However, in the gel the motion remained isotropic. After the first crystallites were formed, polarization transfer from organic protons to silicon became effective owing to the reduced motion of TPA in the MFI framework (173).

Molecular mechanics energy minimization has been carried out on 160 organic structure-directing agents known to form 27 framework types (174). The molecular principal axes of inertia of these molecules were plotted to produce three-dimensional shape–space diagrams. Organic molecules that direct a given zeolite tended to cluster together, suggesting that they were encapsulated in a similar manner. Such studies may have predictive value in designing organic replacements (174). Spectroscopic and microscopic techniques are making it possible to examine at a molecular level the changes occurring during crystal growth (175).

The following conclusions can be made from these studies:

An organic–inorganic composite of template-silicate species formed via favorable hydrophobic contacts has been suggested to aggregate to form the early stages of nuclei.

There is evidence that organic molecules may be trapped in silicate species at the early stages of crystallization. This process is then followed by bond rearrangements to form crystals.

VII. CONCLUSIONS

Several conclusions emerge from this review of the growth of MFI structures. Probably the most interesting is the special role TPA plays in stabilizing the MFI structure, which has been the subject of many studies. As we have noted, this is due to a combination of several factors—charge, hydrophobicity, geometry, which all lead to energetically favorable associations between aluminosilicate (silicate) anions and TPA and promote nuclei formation. Even a simple substitution of one of the propyl groups by -H or $-CH_2OH$ is enough to disrupt the favorable interactions for nuclei formation and limits the composition under which MFI can be made. Altering the length of the alkyl chain, making it smaller (as in TEA) or longer (as in TBA), disrupts nucleation. In TEA, the stabilizing effects of the organic–aluminosilicate interactions are less than TPA, whereas with TBA, the chains are too long and lead to repulsive

interactions between adjacent TBA molecules, thereby disrupting nucleation. It is true that MFI framework can be made in the presence of a large number of organics, including amines, but in all of these cases the composition range is limited in comparison with TPA. These organics typically manifest their crystallization promotion effects via hydrophobic effects, charge neutralization and favorable organic–inorganic interactions (manifested as pore filling). Organics can also be used as the solvent or via a vapor phase.

It is possible to crystallize MFI in the absence of all organics, but the presence of sodium ions and very narrow reactant compositions is required. Again, the presence of TPA allows the use of different inorganic ions, but the effect of the inorganic ions with TPA seems to be primarily manifested on the crystal growth dynamics and morphology. It appears that TPA still controls nucleation, but crystal growth is modified in the presence of inorganic cations and could arise from electrostatic effects related to surface charge. The accelerating effect of oxyanions on MFI growth could also stem from modifications to surface charge.

From a compositional point of view, there appears to be an optimal hydroxide concentration, that keeps the balance between growth and dissolution. Similar observations have been made with F^- as the mineralizing agent.

Other variables of synthesis that have been examined are temperature and seeding. The primary effect of increasing temperature on crystallization is to decrease nucleation time, increase crystallization rate, and decrease particle number densities. More subtle effects are altered morphology due to differing activation energies for different crystal faces.

Seeded systems can promote nucleation by providing small fragments that act as nucleation sites. Larger seed crystals merely act as substrate providing a support for nucleation of randomly oriented crystallites, which typically overwhelm any growth of the seed crystal, especially in concentrated solutions. Thus, in a seeded system, the important species are small (probably nanometer sized) units that are released from the seed and commence growth. For larger crystals to have any effect, attrition from the seed crystals must take place. How the small fragments provide the nuclei for crystal growth is unclear. The two possibilities are that the fragments themselves grow or the dissolution products of the fragments provide the nucleation units.

ZSM-5 crystals are found with very different Si, Al profiles in the crystal. Depending on the use of TPA or Na^+, the Al distribution in ZSM-5 is enriched at the rim or uniform throughout the crystal, respectively. This indicates that for the TPA system, the nuclei and crystals at the early stages of synthesis are more siliceous, probably because of the large size of TPA in comparison with Na^+. Even though there is no upper limit to the Si/Al ratio of MFI (silicalite, Si/Al = ∞), there is an experimental lower limit of 11 and ascribed to Al sitting in a four-membered ring. The comparable mineral with MFI structure has a Si/Al ratio of 7.6 and has not yet been made in the laboratory.

The MFI structure can exist in very large single crystals (0.5 mm) as well as nanocrystals ($\sim$100 nm). Large crystals have made it possible to obtain excellent structural analysis, including the sitting of TPA at channel intersections. Nanocrystals are revolutionizing procedures for making zeolitic membranes via secondary growth processes.

MFI frameworks can be made with very different morphologies, controlled primarily by reactant compositions. A general rule is that larger crystals are obtained if the concentration of the structure-directing agent or hydroxide ion is reduced, since both lead to fewer nuclei. Addition of monovalent inorganic ions also modifies the morphology, with NH_4^+ leading to the largest crystals. Aggregation can be avoided by controlling Si/Al ratios, with higher Si/Al ratios leading to fewer nuclei.

Modeling of zeolite growth has led to several insights into the crystallization process. Of particular interest is the autocatalytic nucleation model, which suggests that the amorphous gel

provides well-formed nuclei upon dissolution and that these structures are located preferentially on the outer surfaces of the amorphous gel. This scenario would suggest that gel restructuring at the surface is influenced by solution species as the proper "nuclei" structures form, and that dissolution of these units occurs in a specific fashion that maintains their integrity. Several studies have shown the presence of amorphous gel exhibiting zeolite-like properties at the beginning of crystallization. Solid-state transformations that preserve the shape of the starting solid into MFI structure is also possible via use of reagents (water, structure-directing agents, SiF_4) through the vapor phase. Restructuring to form crystals possibly involves local dissolution of the solid phase.

In situ studies of change in crystallite size as a function of time indicate the presence of an induction period required for nuclei to form and reach a critical size followed by a linear crystal growth process. The important role of solution species toward surface reaction–controlled crystal growth has been pointed out, and zoned composition of crystals has been correlated with changing solution composition during crystallization.

Considerable research has been done in identifying the molecular precursors that may be relevant to crystal formation. It has been proposed that interactions between silicate species and organics driven by hydrophobic forces can lead to stabilization of specific structures followed by linkage of the silicate units to form nuclei. X-ray scattering has provided dimensions of nanoparticulates that exist at the early stages of synthesis. It was proposed that $\sim$2.8-nm particles upon aggregation formed $\sim$10-nm particles, which were the viable nuclei. The most recent studies suggest the presence of nanoslabs ($1.3 \times 4.0 \times 4.0$ nm^3) formed by aggregation of specific "trimer" structures. These nanoslabs were proposed to aggregate in a specific geometry to form crystals. Another group has proposed cylindrical (8×14 nm^2) units that aggregate and via surface reconstruction form crystals.

The aggregation mechanism can be contrasted with the more commonly accepted process in which the crystal growth occurs by incorporation of solution species. From an overall perspective, it is interesting to contrast how the two growth processes explain some of the experimental results discussed in this review. How would the aggregation process need to be modified for the composition zoning observed in ZSM-5? The aggregation model can probably explain the influence of cations on morphology, since the cations would modify the surface charge and thereby promote or inhibit aggregation. Aggregation would also explain why it is difficult to grow large seed crystals further, where solution-based methods would predict such crystal growth. It is unclear how well the aggregation model can be applied to gel-based synthesis. The possibility that small fragments are released from the gel and aggregate to form nuclei exists. Activation energies for growth along different faces of the crystal are predicted to be different from both models.

In summary, this review of MFI crystallization shows that there can be a tremendous diversity of crystallization conditions leading to crystals of different composition, properties, and morphology. Our understanding of the specific reasons why changes occur is limited, though it is also clear that the huge empirical base that is developed is useful for formulating correlations. The difficulty with zeolite synthesis is that predictions are still difficult and constitute one of the main challenges that lie ahead.

REFERENCES

1. EN Coker, JC Jasen, JA Martens, PA Jacobs, F DiRenzo, F Fajula, A. Sacco Jr. Micropor Mesopor Mater 23:119–136, 1998.
2. DW Breck. Zeolite Molecular Sieves. New York: Wiley, 1974.
3. B Tezak. Disc Faraday Soc 42:175–186, 1966.

4. EM Flanigen. ACS Adv Chem Ser 121:119–139, 1973.
5. RJ Argauer, GR Landolt. US Patent 3702886 (1972).
6. DH Olson, GT Kokotallo, SL Lawton, WM Meier. J Phys Chem 85:2238–2243, 1981.
7. GT Kokotailo, SL Lawton, DH Olson, WM Meier. Nature 272:437–438, 1978.
8. H Lermer, M Draeger, J Steffen, KK Unger. Zeolites 5:131–134, 1985.
9. K-J Chao, J-C Lin, Y Wang, G H Lee. Zeolites 6:35–38, 1986.
10. G Vezzalini, S Quartieri, E Galli, A Alberti, G Cruciani, A Kvick. Zeolites 19:323–325, 1997.
11. EM Flanigen. Pure Appl Chem 52:2191–2211, 1980.
12. EM Flanigen, JM Bennett, RW Grose, JP Cohen, RL Patton, RM Kirchner, JV Smith. Nature 271:512–516, 1978.
13. JM Newsam. In: AK Cheetham, P Day, eds. Solid State Chemistry: Compounds. New York: Oxford University Press, 1992, pp. 234–280.
14. MM Helmkamp, ME Davis. Annu Rev Mater Sci 25:161–192, 1995.
15. ME Davis, RF Lobo. Chem Mater 4:756–768, 1992.
16. A Culfaz, LB Sand. ACS Adv Chem Ser 121:140–151, 1973.
17. VP Shiralkar, A Clearfield. Zeolites 9:363–370, 1989.
18. R Aiello, F Crea, A Nastro, C Pellegrino. Zeolites 7:549–553, 1987.
19. A Erdem, LB Sand. J Catal 60:241–256, 1979.
20. BM Lowe, JRD Nee, JL Casci. Zeolites 14:610–619, 1994.
21. FJ Cachado, CM Lopez, MA Centteno, C Urbina. Appl Catal A 181:29–38, 1999.
22. F Crea, R Aiello, A Nastro, JB Nagy. Zeolites 11:521–527, 1991.
23. U Mueller, KK Unger. Zeolites 8:154–156, 1988.
24. JB Nagy, P Bodart, H Collette, C Fernandez, Z Gabelica, A Nastro, R Aiello. J Chem Soc Faraday Trans I 85:2749–2769, 1989.
25. Z Gabelica, EG Derouane, N Blom. Appl Catal 5:109–117, 1983.
26. S Mintova, V Valtchew, I Kanev. Zeolites 13:102–106, 1993.
27. Z Gabelica, N Blom, EG Derouane. Appl Catal 5:227–248, 1983.
28. A Nastro, LB Sand. Zeolites 3:57–62, 1983.
29. EA Tsokanis, R W Thompson. Zeolites 12:369–373, 1992.
30. M Ghamami, LB Sand. Zeolites 3:155–162, 1983.
31. DM Bibby, NB Milestone, LP Aldridge. Nature 285:30–31, 1980.
32. K-J Chao, TC Tasi, M-S Chem. J Chem Soc Faraday Trans I 77:547–555, 1981.
33. R Kumar, P Mukherjee, RD Pandey, P Rajmohanan, A Bhaumik. Micropor Mesopor Mater 22:23–31, 1998.
34. T Sano, F Mizukami, M Kawamura, H Takaya, T Mouri, W Inaoka, Y Toida, M Watanabe, K Toyoda. Zeolites 12:801–805, 1992.
35. J Warzywoda, N Bac, GA Rossetti Jr., N van der Puil, JC Jansen, H cvan Bekkum, A Sacco Jr. Micropor Mesopor Mater 38:423–432, 2000.
36. BM Lok, TR Cannan, CA Messina. Zeolites 3:282–291, 1983.
37. SL Lawton, WJ Rohrbaugh. Science 247:1319–1322, 1990.
38. F Testa, F Crea, A Nastro, R Aiello, R Mostowicz, JB Nagy. Zeolites 11:633–638, 1991.
39. F Testa, R Szostak, R Chiappetta, R Aiello, A Fonseca, JB Nagy. Zeolites 18:106–114, 1997.
40. V Shen, AT Bell. Micropor Mesopor Mater 7:187–199, 1996.
41. A Chatterjee, R Vetrivel. J Chem Soc Faraday Trans 91:4313–4319, 1995.
42. E de Vos Burchart, H van Koningsveld, B van de Graaf. Micropor Mesopor Mater 8:215–222, 1997.
43. K Tsuji, ME Davis. Micropor Mesopor Mater 11:53–64, 1997.
44. J Patarin, M Soulard, H Kessler, JL Guth, M Diot. Thermochim Acta 146:21–38, 1989.
45. AV Goretsky, LW Beck, SI Zones, ME Davis. Micropor Mesopor Mater 28:387–393, 1999.
46. EW Valyocsik, LD Rollmann. Zeolites 5:123–125, 1985.
47. S Mintova, V Valtchev. Zeolites 13:299–304, 1993.
48. A Araya, BM Lowe. Zeolites 6:111–118, 1986.
49. C Falamaki, M Edrissi, M Sohrabi. Zeolites 19:2–5, 1997.
50. FJ van der Gaag, JC Jansen, H van Bekkum. Appl Catal 17:261–271, 1985.

51. SG Fegan, BM Love. J Chem Soc Faraday Trans I 82:801–814, 1986.
52. KR Franklin, BM Lowe. Zeolites 8:501–507, 1988.
53. J Patarin, M Soulard, H Kessler, J-L Guth, J Baron. Zeolites 9:397–404, 1989.
54. KR Franklin, B M Lowe. Zeolites 8:508–516, 1988.
55. KR Franklin, BM Lowe. Zeolites 8:495–500, 1988.
56. A Araya, BM Lowe. J Chem Soc Chem Commun 1455–1456, 1987.
57. S Mintova, V Valtchev, E Vultcheva, S Veleva. Zeolites 12:210–215, 1992.
58. VP Shiralkar, PN Joshi, MJ Eapen, BS Rao. Zeolites 11:511–516, 1991.
59. T Sano, Y Kiyozumi, F Mizukami, A Iwasaki, M Ito, M Watanabe. Micropor Mater 1:353–357, 1993.
60. TAM Twomey, M Mackay, HPCE Kuipers, RW Thompson. Zeolites 14:162–168, 1994.
61. NN Feoktistova, SP Zhdanov, W Lutz, M Bülow. Zeolites 9:136–139, 1989.
62. CS Cundy, BM Lowe, DM Sinclair. Faraday Disc 95:235–252, 1993.
63. BJ Schoeman, J Sterte, J-E Otterstedt. Zeolites 14:568–575, 1994.
64. R Mostowicz, F Crea, JB Nagy. Zeolites 13:678–684, 1993.
65. A Tavolaro, R Mostowicz, F Crea, A Nastro, R Aiello, JB Nagy. Zeolites 12:756–761, 1992.
66. R Aiello, F Crea, E Nigro, F Testa, R Mostoowicz, A Fonseca, JB Nagy. Micropor Mesopor Mater 28:241–259, 1999.
67. D Zhao, S Qiu, W Pang. Zeolites 13:478–480, 1993.
68. R Althoff, K Unger, F Schuth. Micropor Mater 2:557–562, 1994.
69. A Fonseca, JB Nagy, JEH-A Asswad, G Demortier, R Mostowicz, F Crea. Zeolites 15:131–138, 1995.
70. W Fan, R Li, J Ma, B Fan, J Cao. Micropor Mater 4:301–307, 1995.
71. Z Daqing, Q Shilun, P Wenqin. J Chem Soc Chem Commun 1313–1314, 1990.
72. GD Price, JJ Pluth, JV Smith, JM Bennett, RL Patton. J Am Chem Soc 104:5971–5977, 1982.
73. NR Forbes, LVC Rees. Zeolites 15:444–451, 1995.
74. NR Forbes, LVC Rees. Zeolites 15:452–459, 1995.
75. F Gatti, E Moretti, M Padovan, M Solari, V Zamboni. Zeolites 6:312–316, 1986.
76. N Kanno, M Miyake, M Sato. Zeolites 14:625–628, 1994.
77. H Qisheng, F Shouhau, X Ruren. J Chem Soc Chem Commun 1486–1487, 1988.
78. X Wenyang, L Jianquan, L Wenyuan, Z Huiming, L Bingchang. Zeolites 9:468–473, 1989.
79. M Matsukata, N Nishiyama, K Veyama. Micropor Mater 1:219–222, 1993.
80. MA Uguina, A de Lucas, F Ruiz, DP Serrano. Ind Eng Chem Res 34:451–456, 1995.
81. W Xu, J Dong, J Li. J Chem Soc Chem Commun 131–132, 1990.
82. W Xu, J Dong, J Li, L Li, F Wu. J Chem Soc Chem Commun 755–756, 1990.
83. M Matsukata, N Nishiyama, K Ueyama. Micropor Mater 7:109–117, 1996.
84. SG Thoma, TM Nenoff. Micropor Mesopor Mater 41:295–305, 2000.
85. J Dong, T Dou, X Zhao, L Gao. J Chem Soc Chem Commun 1056–1058, 1992.
86. E Narita, K Sato, T Okabe. Chem Lett 1055–1058, 1984.
87. E Costa, MA Uguina, A de Lucas, J Blanes. J Catal 107:317–324, 1987.
88. LY Hou, RW Thompson. Zeolites 9:526–530, 1989.
89. J Warzywoda, RD Edelman, RW Thompson. Zeolites 11:318–324, 1991.
90. RD Edelman, DV Kukalkar, T Ong, J Warzywoda, RW Thompson. Zeolites 9:496–502, 1989.
91. JB Loos. Zeolites 18:278–281, 1997.
92. CS Cundy, MS Henty, RJ Plaisted. Zeolites 15:353–372, 1995.
93. CS Cundy, MS Henty, RJ Plaisted. Zeolites 15:400–407, 1995.
94. CS Cundy, RJ Plaisted, JP Zhao. Chem Commun 1465–1466, 1998.
95. KR Franklin, BM Lowe. Zeolites 7:135–142, 1987.
96. MH Kim, HX Li, ME Davis. Micropor Mater 1:191–200, 1993.
97. W Xu, JX Dong, J Li, J Ma, T Dou. Zeolites 12:299–305, 1992.
98. E Kikuchi, K Yamashita, S Hiromoto, K Ueyama, M Matsukata. Micropor Mater 11:107–116, 1997.
99. M Salou, F Kooli, Y Kiyozumi, F Midamizu. J Mater Chem 11:1476–1481, 2001.
100. R von Ballmoos, WM Meier. Nature 289:782–783, 1981.

101. R Althoff, BS-Dobrick, F Schüth, K Unger. Micropor Mater 1:207–218, 1993.
102. B Burger, KH-Santo, M Hunger, J Weitkamp. Chem Eng Technol 23:322–324, 2000.
103. A E Persson, B J Schoeman, J Sterte, J-E Otterstedt. Zeolites 14:557–567, 1994.
104. AE Persson, BJ Schoeman, J Sterte, J-E Otterstedt. Zeolites 15:611–619, 1995.
105. R Van Grieken, JL Sotelo, JM Menendez, J A Melero. Micropor Mesopor Mater 39:135–147, 2000.
106. CJH Jacobsen, C Madsen, J Houzvicka, I Schmidt, A Carsson. J Am Chem Soc 122:7116–7117, 2000.
107. J Kornatowski. Zeolites 8:77–78, 1988.
108. EL Wu, SL Lawton, DH Olson, AC Rohrman Jr., GT Kokotailo. J Phys Chem 83:2777–2781, 1979.
109. H van Koningsveld, JC Jansen, H van Bekkum. Zeolites 10:235–242, 1990.
110. G Debras, A Gourgue, J B Nagy, G D Clippeleir. Zeolites 5:369–376, 1985.
111. H van Koingsveld, J C Jansen, H van Bekkum. Zeolites 7:564–568, 1987.
112. CA Fyfe, H Strobl, GT Kokotailo, GJ Kennedy, GE Barlow. J Am Chem Soc 110:3373–3380, 1988.
113. H van Koningsveld, H van Bekkum, JC Jansen. Acta Crystallogr B43:127–132, 1987.
114. Y Yokomori, S Idaka. Micropor Mesopor Mater 28:405–413, 1999.
115. DG Hay, H Jaeger, KG Wilshier. Zeolites 10:571–576, 1990.
116. C Weidenthaler, R X Fischer, R D Shannon, O Medenbach. J Phys Chem 98:12687–12694, 1994.
117. GA Jablonski, LB Sand, JA Gard. Zeolites 6:396–402, 1986.
118. T Bein. Chem Mater 8:1636–1653, 1996.
119. T Sano, Y Kiyozumi, M Kawamura, F Mizukami, H Takaya, T Mouri, W Inaoka, Y Toida, M Watanabe, K Toyoda. Zeolites 11:842–845, 1991.
120. T Sano, F Mizukami, H Takaya T Mouri, M Watanabe. Bull Chem Soc Jpn 65:146–154, 1992.
121. V Valtchev, S Mintova, L Konstantionov. Zeolites 15:679–683, 1995.
122. S Mintova, V Valtchev, L Konstantinov. Zeolites 17:462–465, 1996.
123. JG Tsikoyiannis. WO Haag. Zeolites 12:126–130, 1992.
124. MW Anderson, KS Pachis, J Shi, SW Carr. J Mater Chem 2:255–256, 1992.
125. V Valtchew, BJ Schoeman, J Hedlund, S Mintova, J Sterte. Zeolites 17:408–415, 1996.
126. S Mintova, J Hedlund, V Valtchev, BJ Schoeman, J Sterte. J Mater Chem 8:2217–2221, 1998.
127. A Gouzinis, M Tsapatsis. Chem Mater 10:2497–2504, 1998.
128. J Hedlund. J Por Mater 7:455–464, 2000.
129. V Valtchev, S Mintova. Micropor Mesopor Mater 43:41–49, 2001.
130. M Otake. Zeolites 14:42–52, 1994.
131. CS Gittleman, AT Bell, CJ Radke. Micropor Mater 2:145–158, 1994.
132. R Mostowicz, LB Sand. Zeolites 3:219–225, 1983.
133. F Crea, A Nastro, J B Nagy, R Aiello. Zeolites 8:262–267, 1988.
134. SG Fegan, BM Lowe. J Chem Soc Faraday Trans I 82:785–799, 1986.
135. DT Hayhurst, A Nastro, R Aiello, F Crea, G Giordano. Zeolites 8:416–422, 1988.
136. K Suzuki, Y Kiyozumi, S Shin, K Fujisawa, H Watanabe, K Saito, K Noguchi. Zeolites 6:290–298, 1986.
137. C Janssens, PJ Grobet, RA Schoonheydt, JC Jansen. Zeolites 11:184–191, 1991.
138. H Nakamoto, H Takahashi. Chem Lett 1739–1742, 1981.
139. S Ahmed, MZ El-Faer, MM Abdillahi, MAB Siddiqui, SAI Barri. Zeolites 17:373–380, 1996.
140. R-F Xiao, JID Alexander, F Rosenberger. Faraday Discuss 95:85–95, 1993.
141. RW Thompson, A Dyer. Zeolites 5:202–210, 1985.
142. J Warzywoda, RD Edelman, RW Thompson. Zeolites 9:178–192, 1989.
143. G Golemme, A Nastro, JB Nagy, B Suboti, F Crea, R Aiello. Zeolites 11:776–783, 1991.
144. RW Thompson. Zeolites 12:837–840, 1992.
145. S Gonthier, L Gora, I Güray, RW Thompson. Zeolites 13:414–418, 1993.
146. JD Cook, RW Thompson. Zeolites 8:322–326, 1988.
147. CS Cundy, MS Henty, RJ Plaisted. Zeolites 15:342–352, 1995.
148. M Padovan, G Leofanti, M Solari, E Moretti. Zeolites 4:295–299, 1984.
149. B M Lowe. Zeolites 3:300–305, 1983.
150. O Regev, Y Cohen, E Kehat, Y Talmon. Zeolites 14:314–319, 1994.

151. A Iwasaki, M Hirata, I Kudo, T Sano, S Sugawara, M Ito, M Watanabe. Zeolites 15:308–314, 1995.
152. CS Cundy, BM Lowe, DM Sinclair. J Cryst Growth 100:189–202, 1990.
153. PA Jacobs, EG Derouane, J Weitkamp. J Chem Soc Chem Commun 591–593, 1981.
154. Z Gabelica, J B Nagy, G Debras. J Catal 84:256–260, 1983.
155. PK Dutta, M Puri. J Phys Chem 91:4329–4333, 1987.
156. S Mintova, B Mihailova, V Valtchev, L Konstantinov. J Chem Soc Chem Commun 1791–1792, 1994.
157. G Coudurier, C Naccache, J C Vedrine. J Chem Soc Chem Commun 1413–1415, 1982.
158. KH Yi, SK Ihm. Micropor Mater 1:115–122, 1993.
159. H Dokter, H F van Garderen, TPM Beelen, RA van Santen, W Bras. Angew Chem Inter Ed Engl 34:73–75, 1995.
160. P-PEA de Moor, TPM Beelen, RA van Santen. J Phys Chem B 103:1639–1650, 1999.
161. P-PEA de Moor, TPM Beelen, BUKomanschek, LW Beck, P Wagner, M E Davis, R A van Santen. Chem-Eur J 5:2083–2088, 1999.
162. LE Iton, F Trouw, T O Brun, JE Epperson, JW White, S J Henderson. Langmuir 8:1045–1048, 1992.
163. WH Dokter, TPM Beelen, HF van Garderen, RA van Santen, W Bras, GE Derbyshire, GR Mant. J Appl Crystallogr 27:901–906, 1994.
164. R Ravishankar, CEA Kirschhock, P-P Knops-Gerrits, EJP Feijen, PJ Grobet, P Vanoppen, FCD Schryver, G Miehe, H Fuess, BJ Schoeman, PA Jacobs, JA Martens. J Phys Chem B 103:4960–4964, 1999.
165. EAK Christine, R Ravishankar, F Verspeurt, PJ Grobet, PA Jacobs, JA Martens. J Phys Chem B 103:4965–4971, 1999.
166. CEA Kirschhock, R Ravishankar, LV Looveren, PA Jacobs, JA Martens. J Phys Chem B 103:4972–4978, 1999.
167. CEA Kirschhock, R Ravishankar, PA Jacobs, JA Martens. J Phys Chem B 103:11021–11027, 1999.
168. EJJ Groenen, AGTG Kortbeek, M Mackay, O Sudmeijer. Zeolites 6:403–411, 1986.
169. CTG Knight. Zeolites 10:140–144, 1990.
170. CS Gittleman, SS Lee, AT Bell, CJ Radke. Micropor Mater 3:511–530, 1995.
171. SL Burkett, ME Davis. Chem Mater 7:920–928, 1995.
172. SL Kurkett, ME Davis. J Phys Chem 98:4647–4654, 1994.
173. R Gougeon, L Delmotte, D Le Nouen, Z Gabelica. Micropor Mesopor Mater 26:143–151, 1998.
174. RE Boyett, AP Stevens, MG Ford, PA Cox. Zeolites 17:508–512, 1996.
175. DP Serrano, S van Grieken. J Mater Chem 11:2391–2407, 2001.